

Full Length Articles

The emergence of abnormal hypersynchronization in the anatomical structural network of human brain

Boyuan Yan*, Peng Li

Department of Electrical and Computer Engineering, Texas A&M University, College Station, TX 77843, USA

ARTICLE INFO

Article history:

Accepted 12 September 2012

Available online xxx

Keywords:

Global synchronization

Brain structural connectivity

Spike-wave discharges

ABSTRACT

Brain activity depends on transient interactions between segregated neuronal populations. While synchronization between distributed neuronal clusters reflects the dynamics of cooperative patterns, the emergence of abnormal cortical hypersynchronization is typically associated with spike-wave discharges, which are characterized by a sudden appearance of synchronous around 3 Hz large amplitude spike-wave discharges of the electroencephalogram. While most existing studies focus on the cellular and synaptic mechanisms, the aim of this article is to study the role of structural connectivity in the origin of the large-scale synchronization of the brain. Simulating oscillatory dynamics on a human brain network, we find the space-time structure of the coupling defined by the anatomical connectivity and the time delays can be the primary component contributing to the emergence of global synchronization. Our results suggest that abnormal white fiber connections may facilitate the generation of spike-wave discharges. Furthermore, while neural populations can exhibit oscillations in a wide range of frequency bands, we show that large-scale synchronization of the brain only occurs at low frequencies. This may provide a potential explanation for the low characteristic frequencies of spike-wave discharges. Finally, we find the global synchronization has a clear anterior origin involving discrete areas of the frontal lobe. These observations are in agreement with existing brain recordings and in favor of the hypothesis that initiation of spike-wave discharges originates from specific brain areas. Further graph theory analysis indicates that the original areas are highly ranked across measures of centrality. These results underline the crucial role of structural connectivity in the generation of spike-wave discharges.

© 2012 Published by Elsevier Inc.

Introduction

Normal brain function requires the dynamic interaction of functionally specialized but widely distributed cortical regions. Long-range synchronization of oscillatory signals has been suggested to mediate these interactions within large-scale cortical networks by dynamically establishing task-dependent networks of cortical regions (Varela et al., 2001). Disturbances of such synchronized networks have been implicated in several brain disorders, such as schizophrenia, autism, epilepsy, Alzheimer's disease, and Parkinson's disease (Uhlhaas and Singer, 2006). Especially, while synchronization between distributed neuronal clusters reflects the dynamics of cooperative patterns, the emergence of abnormal cortical hypersynchronization is typically associated with the occurrence of ~3 Hz spike-wave discharges (SWD) recorded on the electroencephalogram (EEG). The sudden appearance of SW patterns from a normal background leads to the traditional concept of sudden hypersynchronous and widespread activity during generalized seizures.

The mechanisms underlying spike-wave patterns are complex and may involve cerebral cortex and thalamus, intrinsic properties of neurons, and various types of synaptic receptors present in the circuit. There has

been notable effort devoted to understanding seizure dynamics and various hypotheses have been proposed to explain the underlying mechanisms (Lyttton, 2008; Yan and Li, 2011). Some studies (Destexhe, 1998; Destexhe et al., 1996, 1998; Giaetta et al., 1987; Pollen, 1964) demonstrate that synaptic receptors are especially important in the generation of epileptic seizures while others believe intrinsic properties of neurons play an important role (de Curtis et al., 1998; Dichter and Ayala, 1987; Halliwell, 1986; Schwindt et al., 1988; Timofeev and Steriade, 2004; Timofeev et al., 2004; Wong and Prince, 1978). While those studies shed light on the intrinsic and synaptic mechanisms of seizure generation, they do not take into consideration the structural connectivity, which may play an important role in the emergence of global synchronization.

Traditionally, the abnormality of structural connectivity is often explored in a localized pathologic brain region, which is typically the focus of partial seizures. For example, in (Dyhrfeld-Johnsen et al., 2007; Santhakumar et al., 2005), the abnormal structural changes (mossy fiber sprouting, mossy cell death, etc) in dentate gyrus are studied to explore the genesis of temporal lobe epilepsy. Recently, the role of structural connectivity underlying generalized epilepsies has received more and more attention. From computational perspectives, in (Benjamin et al., 2012), a phenomenological model of seizure initiation is used to demonstrate that network structure (identified from EEG) in patients with idiopathic generalized epilepsies correlates with smaller

* Corresponding author.

E-mail addresses: byan@tamu.edu (B. Yan), pli@tamu.edu (P. Li).

escape times relative to network structures from controls, suggesting that network structure may play an important role in seizure initiation and seizure frequency. Using the same model, the study in (Terry et al., 2012) demonstrates that EEG discharge representing either generalized or focal seizure arises purely as a consequence of subtle changes in network structure, without the requirement for any localized pathological brain region. In (Goodfellow et al., 2011), the authors show that in an extended local area of cortex, spatial heterogeneities in a model parameter can lead to spontaneous reversible transitions from a desynchronized background to synchronous SWD due to intermittency.

While successfully demonstrating the potential role of network structure underlying generalized epilepsies, none of these studies has been done based on the time-space structure of biologically realistic connectivity of human brain. In fact, as explicit time delays are neglected, these studies are restricted to interacting local populations. To explain the emergence of synchronization at large spatial scales ranging up to almost 20 cm, we believe the network structure of the brain should be taken into consideration. The anatomical connections between areas of the brain form a structure network upon which various neural activities unfold. Brain areas are dynamically coupled to one another forming functional networks associated with perception, cognition, and action, as well as during spontaneous activity in the default or resting state. Existing computational studies demonstrate the important role of the characteristic “small-world” structure of the underlying connectivity matrix between different brain areas in the spontaneous emergence of spatio-temporally structured network activities (Cabral et al., 2011; Deco et al., 2009, 2011; Ghosh et al., 2008; Honey et al., 2007, 2009). Especially, recent studies (Cabral et al., 2011; Deco et al., 2009) have revealed that resting state activity (the temporally coherent activity in the absence of an explicit task) is closely related to the underlying anatomical connectivity. During rest, spontaneous blood oxygen level dependent (BOLD) signal is characterized by slow fluctuations (<0.1 Hz) and anti-correlated spatiotemporal patterns. By modeling each brain region as a neural oscillator and simulating in a biologically realistic brain network, the slow fluctuating and anti-correlated spatiotemporal patterns have been linked to fluctuations in the neural activity and synchrony in the gamma range. Especially, the most agreement of the simulated results with the empirically measured results has been found for a set of parameters (coupling, delay, noise, etc) where subsets of brain areas tend to synchronize in clusters while the network is not globally synchronized.

The aim of this article is to study the role of structural connectivity in the mechanistic origin of the large-scale synchronization of the brain, which may relate to the spread of SW epileptic seizure activity. While synchronization phenomenon in large populations of interacting elements has been widely studied in many areas of natural science, mathematics, and social science (Arenas et al., 2008), there has been little work done specifically considering the space-time structure of a biologically realistic cortical network. To reveal the role of brain structural connectivity in the emergence of such global synchronization, we perform a simulation study based on biologically realistic connectivity of brain areas. The structural connectivity was derived from a macroscopic cortico-cortical connectivity network derived from a diffusion-magnetic resonance imaging (MRI) data set using the method in (Zalesky and Fornito, 2009). The connectivity between all brain area pairs is quantified by a connectivity strength matrix and a fiber length matrix. Different from exiting works (Cabral et al., 2011; Deco et al., 2009, 2011; Ghosh et al., 2008; Honey et al., 2007, 2009), in which the neural dynamics at each brain area is modeled by a single neural oscillator (FitzHugh–Nagumo oscillator, Wilson–Cowan oscillator, etc), we use a system of coupled phase oscillators described by Kuramoto (1984) models to represent neural dynamics at each local brain area. Therefore, the proposed model is capable of representing not only the synchronization on a global level but also the local synchronization on different brain areas.

Specifically, to take into consideration the interplay of local and global processes at different time scales, we use local coupling strength, global coupling strength, time delay, and intrinsic frequency as independent parameters. An extensive exploration of the parameter space illustrates that the space-time structure of the coupling defined by the anatomical connectivity and the time delays can be the primary component contributing to the emergence of global synchronization. Our results will show that the global synchronization is highly dependent on the time delays and the intrinsic frequencies of the oscillators. To highlight the crucial role of interrelationship between local processes and the global activity, we further characterize the initialization of synchronization in both time and space. Our results will demonstrate that the initialization of global synchronization has a clear anterior origin involving discrete areas of the frontal lobe. While experimental observations of frontal epileptic focus do exist (Amor et al., 2009; Holmes et al., 2004; Pavone and Niedermeyer, 2000), there is a lack of understanding of the underlying mechanism. In this paper, by performing graph theory analysis of the structural connectivity, we will point out that the initialized areas of global synchronization (“hot spots”) correspond to the nodes with highest degree of centrality (“structural hubs”). This once again underscores the crucial role of structural connectivity in the generation of SW epileptic seizures.

Methods

Structural connectivity

We use the structural connectivity between 80 cortical areas of the human brain. The areas are divided according to a functional subdivision of the cortex derived from the automated anatomical labeling (AAL) atlas (Tzourio-Mazoyer et al., 2002). The structural data for brain connectivity is provided by Andrew Zalesky and Alex Fornito. The structural connectivity is obtained from a macroscopic cortico-cortical connectivity network derived from a diffusion-magnetic resonance imaging (MRI) data set using the algorithm proposed in (Zalesky and Fornito, 2009).

In (Zalesky and Fornito, 2009), a new DTI-derived measure of cortico-cortical connectivity is established based on the notion of information flow. The measure is intended to reflect the maximum rate at which information can be transmitted between a pair of cortical regions, which is quantified by the net capacity of all interconnecting fiber bundles. The set of all voxels comprising DTI space is first partitioned into two sets: white-matter \mathcal{W} , and grey-matter \mathcal{G} using either manual tracing or any of a number of automated segmentation algorithms. The set \mathcal{G} is then subdivided into N continuous cortical regions according to existing functional subdivision of interest to the researcher. Then, a 3-D lattice scaffolding for white-matter is constructed by drawing a link between each pair of voxels in a 26-voxel neighborhood for which their two respective principal eigenvectors form a sufficiently small angle. Let g_i be the set of voxels comprising cortical region $i = 1, \dots, N$. Let $E(i) \in \mathcal{W}$ denote the set of white-matter voxels comprising the interface cortical region g_i . A path between a pair of nodes u and v is said to be an (i, j) -path if $u \in E(i)$ and $v \in E(j)$. Let $f_{i,j}$ denote the maximum number of link-disjoint (i, j) -paths that can be established. Since the capacity of a fiber bundle is measured as the maximum number of link-disjoint paths that can be established between opposing ends of a fiber bundle, the net capacity provided by all fiber bundles interconnecting cortical region g_i and g_j , given by $f_{i,j}$, is used as a measure of connectivity strength.

The connectivity between all brain area pairs is quantified by two 80×80 matrices: a connectivity strength matrix \mathbf{C} and a fiber length matrix \mathbf{L} . As described above, the connectivity strength is estimated based on the density of the white fiber tracts, which is given by the net capacity of fiber bundles $f_{i,j}$. The length of fiber connecting two brain areas is calculated as the average length across all the fibers connecting them. Both matrices are obtained by averaging over 31

control subjects. Since tractography does not give fiber directionality, both matrices are symmetric.

The human brain is divided into two hemispheres (left and right). There are 41 different anatomical areas in each hemisphere. As each area appears in both hemispheres, the total number is 80. For the same anatomical area in different hemispheres, there are different indices and labels. The list of 41 anatomical areas is given in Fig. 1(C). For

each area, it shows the index and label in the right hemisphere (RH), the index and label in the left hemisphere (LH), the name of the area, and the corresponding anatomical region it belongs to. The connectivity strength matrix **C** and fiber length matrix **L** are shown in Figs. 1(A) and (B), respectively. The connectivity strength is normalized so that the maximal strength is 1 ($\max(C_{pq}) = 1, p, q = 1, \dots, P$), where P is the total number of areas and $P = 80$ for the current model. The intra-area

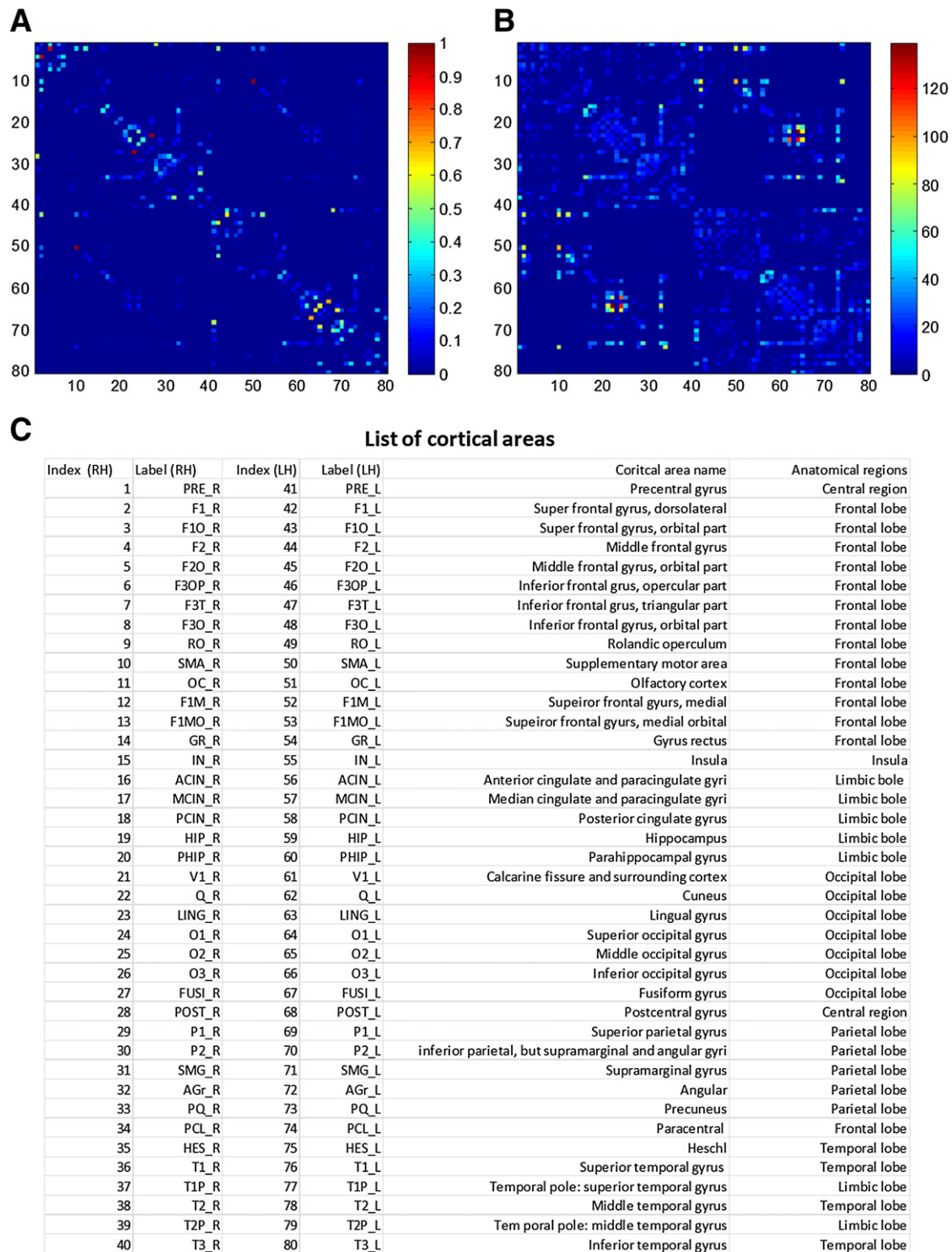


Fig. 1. Structural connectivity of the brain. (A) The connectivity strength matrix (the connectivity strength is normalized so that the maximal strength is 1). (B) The fiber length matrix (mm). (C) The list of anatomical areas of interests. There are 41 different anatomical areas of interests, and each appears in both hemispheres. In the table, each row corresponds to an anatomical area, and the columns show the index and label of the area in the right hemisphere (RH), the index and label of the area in the left hemisphere (LH), the name of the area, and the corresponding anatomical region it belongs to.

connectivity strength and fiber length are set to 0 ($\mathbf{C}_{pp} = 0, \mathbf{L}_{pp} = 0, p = 1, \dots, P$). The order of brain areas in both matrices is arranged according to the index of brain areas in Fig. 1(C).

Graph theory methods

Centrality is a structural attribute of nodes in a network, which measures how central an actor is in network, and the contribution of network position to the importance, influence, prominence of an actor in a network. Central nodes in a network are those that have structural or functional importance. To explore the centrality, we compute two measures for all nodes: degree centrality and betweenness centrality, which have been used to study the structural connectivity of the brain (Ghosh et al., 2008; Honey et al., 2007). In this study, both measures are computed based on the connectivity strength matrix \mathbf{C} .

Degree centrality is defined as the number of links incident upon a node (i.e., the number of ties that a node has). The degree centrality of a brain area is computed based on the connectivity strength matrix \mathbf{C} . As the matrix \mathbf{C} is symmetric, the degree of the p th brain area is computed as the sum of the elements in the p th row $deg_p = \sum_{q=1}^P \mathbf{C}_{pq}, p = 1, \dots, P$.

Betweenness centrality is the fraction of all shortest paths (a path between two nodes in a graph such that the sum of the weights of its constituent edges is minimized) in the network that contain a given node. Nodes with high values of betweenness centrality participate in a large number of shortest paths. The betweenness centrality is calculated by using the Matlab toolbox (<http://www.brain-connectivity-toolbox.net>), which is specially developed for complex network measures of brain connectivity (Rubinov and Sporns, 2010).

Neural dynamics model

We simulate the neural activity on a network of N nodes defined using the previously described structural connectivity: the connection strength matrix \mathbf{C} (normalized so that the maximal strength is 1) and the fiber length matrix \mathbf{L} . For convenience, we first transform the fiber length matrix \mathbf{L} into a conductance delay matrix \mathbf{T} by a choice of a conduction velocity $v = 1$ m/s such that $\mathbf{T} = \mathbf{L}$. As the maximal fiber length in \mathbf{L} is 139 mm, the maximal conductance delay in \mathbf{T} is 139 ms.

Different from exiting works (Cabral et al., 2011; Deco et al., 2009, 2011; Ghosh et al., 2008; Honey et al., 2007, 2009), in which the neural dynamics at each brain area is modeled by a single neural oscillator (FitzHugh–Nagumo oscillator, Wilson–Cowan oscillator, etc), we use a system of coupled phase oscillators described by Kuramoto (1984) models to represent neural dynamics at each local brain area. Therefore, the proposed model is capable of representing not only the synchronization on a global level but also local synchronization on a specific brain area. Synchronization phenomena in large populations of interacting elements have been intensively studied in physical, biological, chemical, and social systems. The Kuramoto model (Acebron, 2005; Kuramoto, 1984) is a successful approach to the problem of synchronization, in which each member of the population is described as a phase oscillator running at arbitrary intrinsic frequencies and those oscillators are coupled through the sine of their phase differences. While simple enough to be mathematically tractable, the model is sufficiently complex to be nontrivial, rich enough to display a large variety of synchronization patterns, and sufficiently flexible to be adapted to many different contexts.

The Kuramoto model has been used to study oscillatory brain activity and several extensions have been proposed that increase its neurobiological plausibility, for instance by incorporating topological properties of local cortical connectivity (Breakspear et al., 2010). In particular, it describes how the activity of a group of interacting neurons can become synchronized and generate large-scale oscillations (Kitzbichler et al., 2009). Simulations using the Kuramoto model with realistic long-range cortical

connectivity and time-delayed interactions reveal the emergence of slow patterned fluctuations that reproduce resting-state BOLD functional maps, which can be measured using fMRI (Cabral et al., 2011).

The dynamics of the Kuramoto model consisting of a population of N coupled phase oscillators is governed by (Acebron, 2005)

$$\dot{\theta}_n(t) = \omega_n + \sum_{j=1}^N k_{nj} \sin(\theta_j(t - \tau_{nj}) - \theta_n(t)), n = 1, \dots, N, \quad (1)$$

where $\theta_n(t)$ is the phase of the n th oscillator at time $t, f_n = \omega_n/2\pi$ is the intrinsic frequency of the n th oscillator, k_{nj} and τ_{nj} are the coupling strength and conductance delay from j th oscillator to n th oscillator.

In this study, we assume all the oscillators have the same intrinsic frequency

$$f_n = f, n = 1, \dots, N, \quad (2)$$

and use f as a global parameter to study the occurrence of synchronization at different frequencies. If the n th oscillator and the j th oscillator are from the p th and the q th brain areas, respectively, then

$$k_{nj} = S_{global} \mathbf{C}_{pq} \quad \tau_{nj} = S_{delay} \mathbf{T}_{pq}, \quad (3)$$

where \mathbf{C}_{pq} and \mathbf{T}_{pq} are the elements of the p th row and q th column of the matrices \mathbf{C} and \mathbf{T} , and S_{global} and S_{delay} are the scaling factors. Therefore, the connectivity and the delay matrices are fixed in their structure and only their scaling can be varied with S_{global} and S_{delay} , respectively. If the two oscillators are from the same brain area, then

$$k_{nj} = S_{local} \quad \tau_{nj} = 0, \quad (4)$$

where S_{local} is the scaling factor for local coupling strength. So each oscillator connects to all other local oscillators within each brain area. As the current study is focused on the role of global connectivity, we assume the local coupling strength is the same for all brain areas and the local time delay is 0.

At the global level, the network synchrony can be evaluated by a complex-valued global order parameter defined by

$$R(t) e^{i\phi(t)} = \frac{1}{N} \sum_{n=1}^N e^{i\theta_n(t)}, \quad (5)$$

where the amplitude $R(t)$ measures phase uniformity and varies between 0 for a fully desynchronized or incoherent state to 1 for a fully synchronized state. For sufficient synchrony, the phase $\phi(t)$ describes the movement of the oscillator ensemble around the unit circle.

At the local level, the network synchrony for each brain area can be evaluated similarly. For example, if there are P brain areas and M oscillators in each area, the local order parameter for the p th area is defined as follows

$$R_p(t) e^{i\phi_p(t)} = \frac{1}{M} \sum_{m=1}^M e^{i\theta_{m(p)}(t)}, p = 1, \dots, P, \quad (6)$$

where $\theta_{m(p)}(t)$ represents the phase of the p th oscillator in the m th brain area. As all the brain areas have the same number of oscillators in the current model, the global parameter is the average of the local order parameters

$$R(t) e^{i\phi(t)} = \frac{1}{P} \sum_{p=1}^P R_p(t) e^{i\phi_p(t)}. \quad (7)$$

The present model depends on four independent parameters: scaling factor of global coupling strength S_{global} , scaling factor of local coupling strength S_{local} , scaling factor of global delay S_{delay} , and intrinsic frequency f . In this work, we conduct a set of partial

parametric studies in the 4 dimensional space ($S_{global}, S_{local}, S_{delay}, f$). We first explore the 3 dimensional subspace ($S_{global}, S_{local}, S_{delay}$) by choosing an intrinsic frequency $f = 4$ Hz. In the first step, we study the role of structural connectivity in the global synchronization in the delta range, which may correspond to the hypersynchronized oscillations in SW epileptic seizures. In the second step, we explore the 3 dimensional subspace (S_{global}, S_{local}, f) by choosing a scaling factor $S_{delay} = 0.1$ for time delays. This scaling factor corresponds to a conduction speed of 10 m/s, which is in the physiologically realistic range of propagation velocity (around 5–20 m/s) for the adult primate brain (Ghosh et al., 2008). In this step, we study the influence of intrinsic frequencies on the global synchronization.

In this study, there are 80 brain areas ($P = 80$) and there are 4 oscillators in each area ($M = 4$). Therefore, the total number of oscillators is 328 ($N = 328$). The system of N dynamical equations was numerically solved with a time-step 0.1 ms using forward Euler scheme. In each simulation, phases of oscillators in each brain area are initialized to be uniformly distributed on the interval $[-\pi, \pi]$. As a result, the amplitudes of the global and local order parameters equal zero $R(0) = 0$, $R_p(0) = 0$, $P = 1, \dots, P$, and the whole network is initialized in a state of fully desynchronized or incoherence.

The simulator is implemented in C++ on a 24-core PowerEdge R715 machine with 2 AMD Operton 2.2 GHz 12-core processors and 32 GB RAM. The simulation results are processed and visualized in Matlab. Especially, the BrainNET Viewer (<http://www.nitrc.org/projects/bnv/>) is used to visualize the brain network.

Results

Identification of the central nodes

Central nodes in a network are those that have structural or functional importance. To explore the centrality, we compute degree centrality and betweenness centrality for all the brain areas (Methods). A brain view of connectivity, degree centrality, and betweenness centrality is shown in Fig. 2(A). The figure includes sagittal, axial, and coronal views of both hemispheres of the brain. The color of nodes represents degree centrality (which decreases from deep red to deep blue) and the size of nodes represents betweenness centrality. The size of edges connecting two nodes represents the strength of connectivity. Degree centrality and betweenness centrality of brain areas are also compared in the bar graphs in Figs. 2(B) and (C), respectively.

The top twenty brain areas for degree centrality and betweenness centrality are listed in Figs. 2(E) and (F), respectively. For degree centrality, the top five areas are right dorsolateral part of superior frontal gyrus (F1_R), left dorsolateral part of superior frontal gyrus (F1_L), left middle occipital gyrus (O2_L), right supplementary motor area (SMA_R), and right middle frontal gyrus (F2_R). For betweenness centrality, the top five areas are left dorsolateral part of superior frontal gyrus (F1_L), right dorsolateral part of superior frontal gyrus (F1_R), left middle frontal gyrus (F2_L), right middle frontal gyrus (F2_R), and right middle temporal gyrus (T2_R).

Among those brain areas, right dorsolateral part of superior frontal gyrus (F1_R), left dorsolateral part of superior frontal gyrus (F1_L), and right middle frontal gyrus (F2_R) are highly ranked across both measures, and can be identified as structural hubs in terms of centrality. Conceptually similar to an airline hub, these are brain areas with a comparatively high number of connections to the rest of the network. As we will demonstrate below, the structural hubs have consequences on the initialization of global synchronization.

Roles of coupling strengths and conduction delays in the emergence of global synchronization

As briefly mentioned in Methods, the present model depends on four free parameters: scaling factor of global coupling strength

S_{global} , scaling factor of local coupling strength S_{local} , scaling factor of global delay S_{delay} , and intrinsic frequency f . In this work, we conduct a set of partial parametric studies in the 4 dimensional space ($S_{global}, S_{local}, S_{delay}, f$).

In this part, we explore the 3 dimensional subspace ($S_{global}, S_{local}, S_{delay}$) by choosing an intrinsic frequency $f = 4$ Hz to study the role of structural connectivity in the global synchronization in the delta range. Such synchronization may correspond to the hypersynchronized oscillations in SW epileptic seizures. The ranges of the three parameters are as follows: $S_{global} \in [0, 1]$, $S_{local} \in [0, 1]$, and $S_{delay} \in [0, 1]$. As a result, in the range of parameters, all coupling strengths are smaller than 1. The range of coupling strengths is selected based on the following two reasons: first, the coupling strength is sufficiently small to make sure the phase reduction remains valid (Breakspear et al., 2010); second, the range is sufficiently large to unveil the roles of parameters of interests qualitatively. The maximal scaling factor of the delay $S_{delay} = 1$ corresponds to the smallest conduction velocity $v = 1$ m/s, and thus the range of delays covers the physiologically realistic range of propagation velocities for the adult primate brain (around 5–20 m/s) (Ghosh et al., 2008). For each set of parameter combination ($S_{global}, S_{local}, S_{delay}$), the whole network is initialized in a fully desynchronized state, and simulated for 10 seconds so that steady state can be approached in most cases. Note that, similar qualitative results can be found by repeating the simulation for different instantiations of the initial conditions. The amplitude of global order parameter at the final moment $R(10)$ is used as the measure of global synchronization.

As shown in Fig. 3, the 3 dimensional parameter space is demonstrated as a set of 2 dimensional plane corresponding to different time delays. In Figs. 3(A)–(F), the scaling factors of time delays are $S_{delay} = 0$ (A), $S_{delay} = 0.1$ (B), $S_{delay} = 0.2$ (C), $S_{delay} = 0.3$ (D), $S_{delay} = 0.4$ (E), and $S_{delay} = 0.5$ (F). The corresponding conduction velocities are $v = 0$ m/s (A), $v = 10$ m/s (B), $v = 5$ m/s (C), $v = 3.33$ m/s (D), $v = 2.5$ m/s (E), and $v = 2$ m/s (F). In Figs. 3(A)–(F), X-axis represents the scaling factor of local coupling strength S_{local} , Y-axis represents the scaling factor of global coupling strength S_{global} , and the color represents the degree of global synchronization. In Figs. 3(A)–(F), we see not only coupling strengths can play an important role in the emergence of global synchronization but also time delays can substantially change the dynamical properties of brain networks.

First, as shown in Figs. 3(A)–(F), the global synchronization is highly dependent on the time delays. In particular, the degree of global synchronization is decreased as the time delay increases. This means time delays tend to break coherence in populations of interacting units. Intuitively, this can be explained as follows: when all the oscillators oscillate in a synchronous fashion at the same frequency, the couplings reinforce synchronous in-phase oscillation without conduction delay; however, if conduction delay becomes nonzero, the stable synchronous oscillation may become unstable because the transmitted signal from one oscillator may arrive during the anti-phase of the other oscillator. Note that, the physiologically realistic range of propagation velocities is around 5–20 m/s for the adult primate brain (Ghosh et al., 2008). Therefore, the results in Figs. 3(B) and (C) fall into this physiological range as $S_{delay} = 0.1$ and $S_{delay} = 0.2$ correspond to $v = 10$ m/s and $v = 5$ m/s, respectively. Our results show that the state of global synchronization does exist in the physiological range and tends to vanish for longer delays $S_{delay} > 0.3$.

Second, the relationship between global synchronization and coupling strength becomes more complex in the presence of time delays. In Fig. 3(A), when there is no delay, the relationship between two coupling strength in terms of global synchronization is straightforward: the global synchronization increases as either global or local coupling strength increases while the other is constant. Intuitively, one might think that an increase of coupling strength will always lead to a higher degree of global synchronization, but this might not be the case when time delays exist. For example, as shown in Figs. 3(B)–(F), the highest degree of global synchronization does not occur when both global and local coupling strength are maximal. In

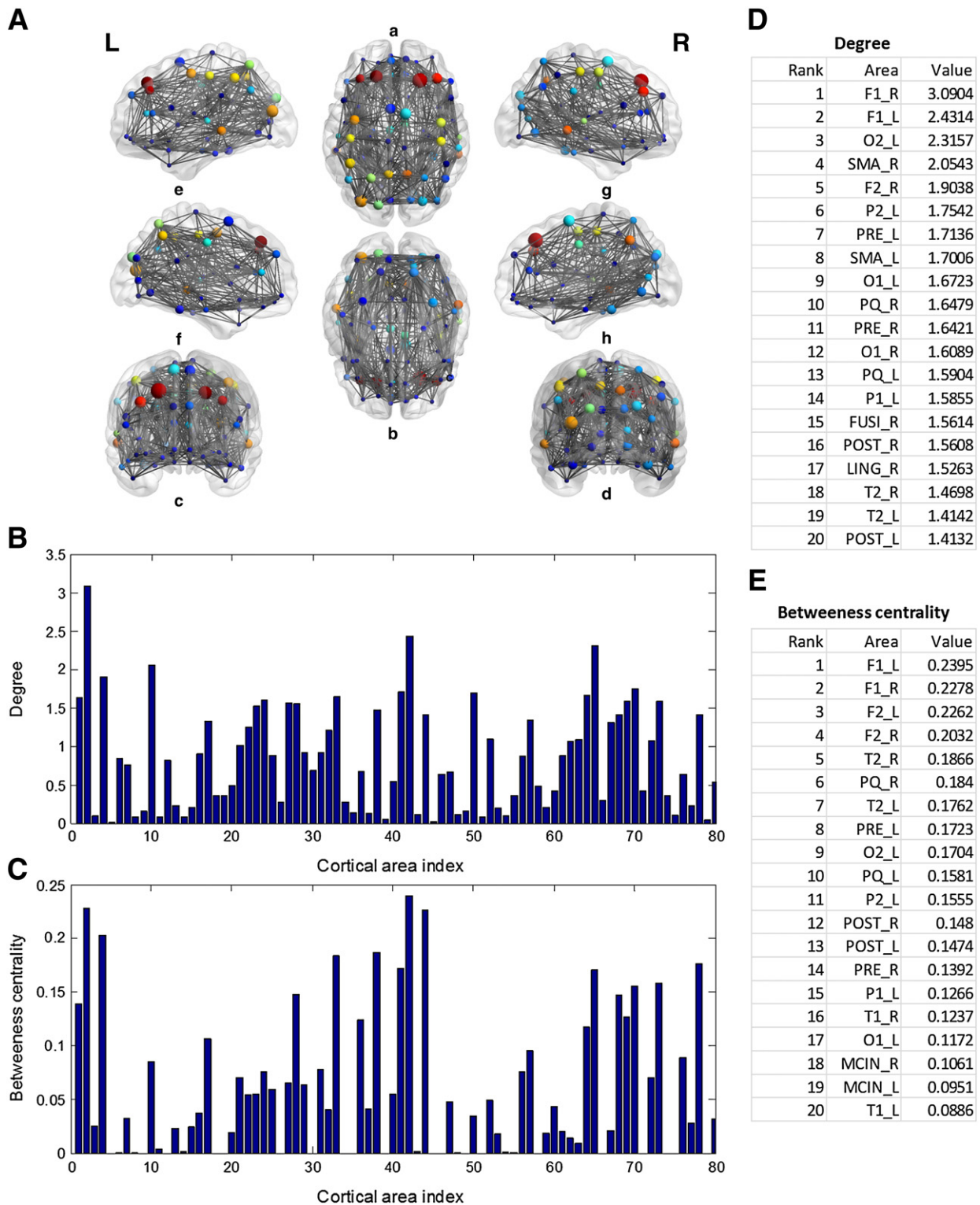


Fig. 2. Degree centrality and betweenness centrality. (A) A brain view of connectivity, degree centrality, and betweenness centrality. The figure includes sagittal, axial, and coronal views of both hemispheres of the brain: (a) axial top to bottom, (b) axial bottom to top, (c) coronal front to back, (d) coronal back to front, (e) sagittal left to right (left hemisphere), (f) sagittal right to left (left hemisphere), (g) sagittal right to left (right hemisphere), (h) sagittal left to right (right hemisphere). The color of nodes represents the degree centrality (which decreases from deep red to deep blue) and the size of nodes represents the betweenness centrality. The size of edges connecting two nodes represents the strength of connectivity. (B) The Y-axis represents degree centrality and the X-axis represents the index of brain area. (C) The Y-axis represents betweenness centrality and the X-axis represents the index of brain areas. (D) Top twenty ranked brain areas for degree centrality. (E) Top twenty ranked brain areas for betweenness centrality. (For interpretation of the references to color in this figure legend, the reader is referred to the web version of the article.)

463 Fig. 3(C), the highest degree of global synchronization occurs in two disjoint sets. In contrast, in Figs. 3(B), (D), (E), and (F), the highest
 464 degree of global synchronization occurs only in one set, in which the
 465 global coupling strength is not maximal.
 466

Overall, these results show that space–time structure of the coupling defined by the anatomical connectivity (space) and the time
 467 delays (time) can be the primary component contributing to the
 468 emergence of global synchronization. Those results may have direct
 469
 470

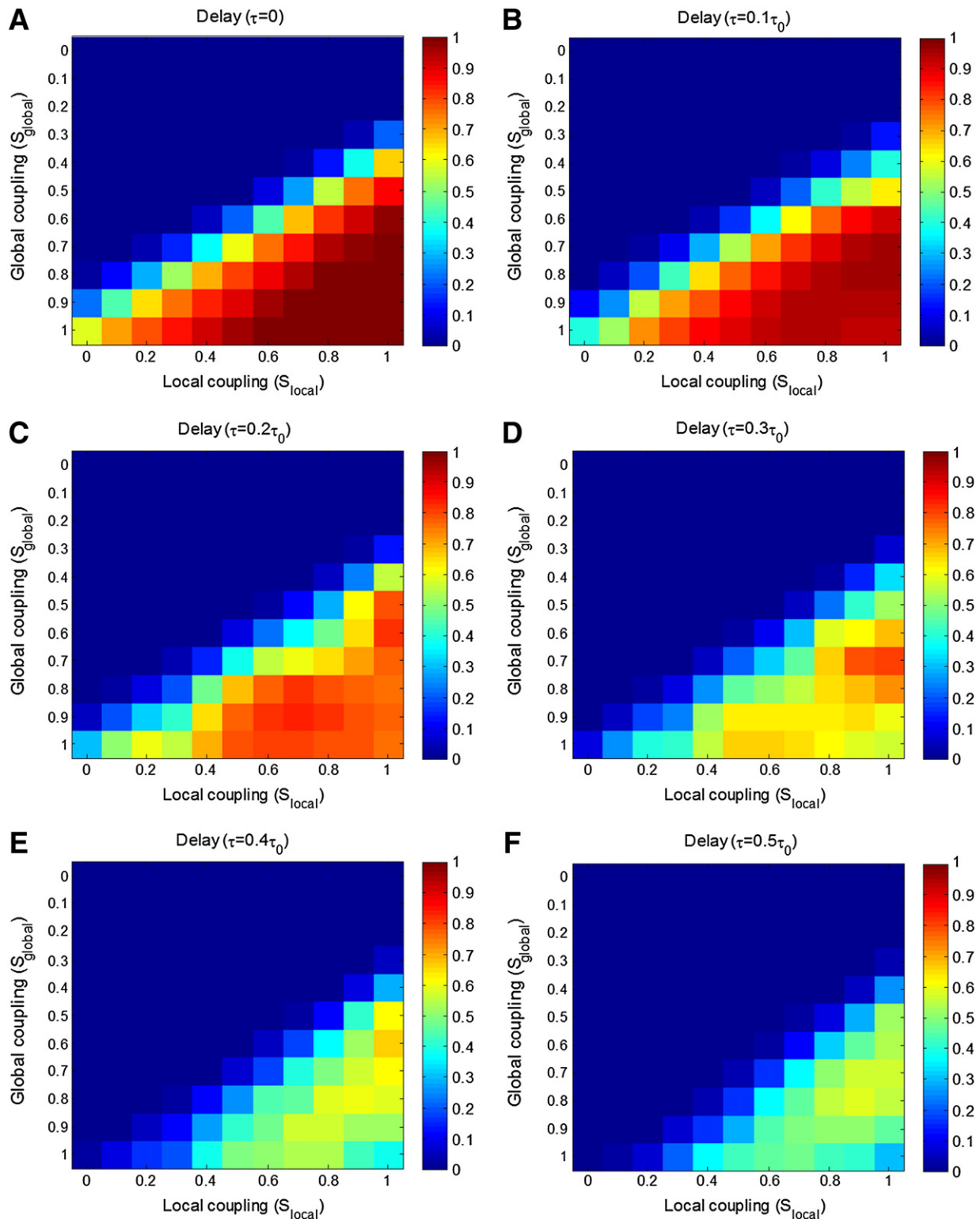


Fig. 3. Global synchronization in the parameter space of global and local coupling strength at different time delays. The X-axis represents the scaling factor of local coupling strength S_{local} , the Y-axis represents the scaling factor of global coupling strength S_{global} , and the color represents the amplitude of global order parameter. (A) Time delay $\tau=0$ ($v=0$ m/s). (B) Time delay $\tau=0.1\tau_0$ ($v=10$ m/s). (C) Time delay $\tau=0.2\tau_0$ ($v=5$ m/s). (D) Time delay $\tau=0.3\tau_0$ ($v=3.33$ m/s). (E) Time delay $\tau=0.4\tau_0$ ($v=2.5$ m/s). (F) Time delay $\tau=0.5\tau_0$ ($v=2$ m/s). (For interpretation of the references to color in this figure legend, the reader is referred to the web version of the article.)

471 implications for studies of SW epileptic seizures. The SW epileptic sei- 476
 472 zures, different from localized seizure, are characterized by a sudden 477
 473 emergence of brain level synchronization. While the roles of cellular 478
 474 and synaptic mechanisms have been widely studied, the sudden 479
 475 emergence of synchronization in such a large scale brain network is

still difficult to explain. In this regard, we hypothesize that the brain 476
 structural connection is possible to play an important role. For exam- 477
 ple, the role of time delays in global synchronization indicates that 478
 the abnormality of white matter might facilitate the emergence of 479
 SW epileptic seizures. The abnormality of the length, diameter, and 480

481 myelination of axons may contribute to the abnormality of the time
482 delays. To verify the hypothesis, computational studies need to be
483 carried out with imaging techniques to quantify white matter integri-
484 ty of the patients suffering from SW epilepsy.

485 *Roles of intrinsic frequencies in the emergence of global synchronization*

486 Mathematically, how important time delays are for a population of
487 coupled phase oscillators is dependent on the ratio of the time delay
488 to the natural period of a typical oscillator. In the scenario of a brain
489 network, an interesting question would be how intrinsic frequencies
490 influence the degree of global synchronization. In other words, can
491 global synchronization emerge at all intrinsic frequencies? To study
492 the role of intrinsic frequency, we explore the 3 dimensional subspace
493 (S_{global} - S_{local} - f) by choosing a scaling factor $S_{delay} = 0.1$. This corre-
494 sponds to a conductance speed of 10 m/s, which is in the physiologi-
495 cally realistic range of propagation velocity (around 5–20 m/s) for the
496 adult primate brain (Ghosh et al., 2008). Similar to the previous case,
497 for each parameter combination (S_{global} - S_{local} - f), the whole network is
498 initialized in a fully desynchronized state, and simulated for 10 s. The
499 amplitudes of global order parameters at $t = 10$ s are used as the mea-
500 sure of global synchronization.

501 As shown in Fig. 4, the 3 dimensional parameter space is demon-
502 strated as a set of 2 dimensional plane corresponding to different in-
503 trinsic frequencies. The intrinsic frequencies in Figs. 4(A)–(F) are
504 2 Hz, 4 Hz, 6 Hz, 8 Hz, 10 Hz, and 12 Hz, respectively. While longer
505 conductance delay tends to break coherence in populations of
506 interacting units, higher intrinsic frequencies have the same effects.
507 The results in Fig. 4 demonstrate a decrease of global synchronization
508 as the intrinsic frequency increases. In particular, global synchroniza-
509 tion tends to emerge at frequencies less than 6 Hz. In Figs. 4(A) and
510 (B), large areas in parameter space are found where a high degree
511 of synchronization can be achieved. Starting from Fig. 4(C), the
512 areas corresponding to high values of global synchronization signifi-
513 cantly decreases. Especially, the global synchronization vanishes be-
514 yond 12 Hz in the parameter space. The observation that global
515 synchronization tends to emerge at low frequencies may partially ex-
516 plain the low characteristic frequencies of SWD. More interestingly,
517 this agrees well with existing experimental observations. While neu-
518 ral populations can exhibit oscillations in a wide range of frequency
519 bands, global synchronization in the brain scale only occurs at low
520 frequencies. Although long range synchronization at high frequencies
521 (beta and gamma rhythms) does exist in separate parts of the brain
522 (Varela et al., 2001), the scale of such synchronization is quite limited
523 compared with the generalized synchronization in SW epileptic seizures.

524 **Cortical local and global synchronization interplay in the** 525 **emergence of global synchronization**

526 In the previous sections, we have demonstrated the roles of cou-
527 pling strength, time delay, and intrinsic frequency in the global syn-
528 chronization of the brain network. Another important question is
529 about the roles played by different brain areas in the initialization of
530 the global synchronization. It is interesting to know whether the
531 global synchronization is initialized from some particular brain
532 areas. To answer this question, we choose a combination of parameter
533 $S_{global} = 1$, $S_{local} = 1$, $S_{delay} = 0.1$ ($v = 10$ m/s), and $f = 4$ Hz to examine
534 the time courses of global and local synchronization. Note that, simi-
535 lar qualitative results can be obtained with other combinations of
536 parameters underlying global synchronization. In this study, we use
537 local order parameters to characterize the local synchronization of
538 each brain area and a global order parameter to characterize the global
539 synchronization.

540 As shown in Fig. 5(A), the blue lines represent the amplitudes of
541 local order parameters of brain areas, and the red line represents the
542 amplitude of the global order parameter. The global synchronization

543 starts from an increase of local synchronization of some brain areas,
544 and increases significantly in hundreds of milliseconds. The time
545 courses of the amplitudes of global and local order parameters agree
546 with the experimental observations in (Amor et al., 2009), where the
547 mean global and local synchronization time course across all 21 seizures
548 is depicted. In terms of local synchronization, there is considerable
549 variation among brain areas: some brain areas tend to get synchronized
550 earlier than others.

551 To better demonstrate the time courses, we show snapshots of
552 global and local order parameters at different times ($t = 0$ s, $t = 4$ s,
553 $t = 5$ s, $t = 6$ s, $t = 7$ s) in the polar coordinate system, where
554 complex-valued order parameter is represented by a vector whose
555 length is $R(t)$ and angle is $\phi(t)$. In Fig. 5(B), at $t = 0$ s, all the order pa-
556 rameters are represented by the origin. This is because the phases of
557 oscillators in each brain area are initialized to be uniformly distribut-
558 ed, and thus the amplitudes of all the order parameters equal zero at
559 the beginning of the simulation. From $t = 4$ s to $t = 7$ s, we take snap-
560 shots every single second to demonstrate the emergence of synchro-
561 nization at both local and global levels. In Fig. 5(C), at $t = 4$ s, the
562 maximal amplitude of local order parameters is only 10^{-5} , and all
563 the brain areas are still fully desynchronized. In Fig. 5(D), at $t = 5$ s,
564 the maximal amplitude of local order parameters is increased to be
565 0.002, and some brain areas start to show a tendency toward local
566 synchronization. Significant changes characterized by local synchro-
567 nization of some brain areas start to occur at $t = 6$ s. As shown in
568 Fig. 5(E), at the local level, a few brain areas are in a state of partial
569 synchronization, and the maximal amplitude of local order param-
570 eters is about 0.5. In contrast, at the global level, the network is still
571 desynchronized as the amplitude of global order parameter is only
572 0.05. By the time $t = 7$ s, as shown in Fig. 5(E), not only many brain
573 areas have become locally synchronized but also the global synchrony
574 level has increased substantially. The amplitude of the global order
575 parameter is 0.66 and the network is partially synchronized at the
576 global level. Overall, the above results show that the emergence of
577 global synchronization starts from the emergence of local synchroni-
578 zation of a few brain areas.

579 Given the observation above, it is interesting to find out what
580 brain areas are involved at the initialization stage of global synchroni-
581 zation and why. To answer this question, we further characterize the
582 initialization of synchronization in both time and space. First of all, we
583 study the spatial distribution of local synchronization events at $t = 6$ s
584 when global synchronization starts to emerge. As shown in Fig. 6(A),
585 a brain view of the degree of local synchronization is given. The figure
586 includes sagittal, axial, and coronal views of both hemispheres of the
587 brain, where the color of nodes represents the amplitude of local
588 order parameter (which decreases from deep red to deep blue), and
589 the size of nodes represents the degree centrality. We see there is a
590 strong correlation between the degree of local synchronization and
591 the degree centrality: the nodes with deep red colors turn out to be
592 the nodes of large sizes. To better demonstrate this, the amplitudes
593 of local order parameters of brain areas are compared in Fig. 6(B),
594 and the top twenty ranked brain areas are listed in Fig. 6(C).

595 In the initialization stage of global synchronization ($t = 6$ s), the top
596 five ranked areas are right dorsolateral part of superior frontal gyrus
597 (F1_R), left dorsolateral part of superior frontal gyrus (F1_L), right sup-
598plementary motor areas (SMA_R), right middle frontal gyrus (F2_R),
599 and left supplementary motor areas (SMA_L). Compared with the lists
600 in Fig. 2(C), we see that the structural hubs identified (F1_R, F1_L,
601 F2_R) are ranked in the first, second, and fourth places, respectively,
602 in Fig. 6(C). This means global synchronization is initialized from
603 a few “hot spots” corresponding to brain areas with highest degree of
604 centrality. According to the anatomical regions defined in (Tzourio-
605 Mazoyer et al., 2002), among the top twenty areas, 17 areas belong
606 to frontal lobe: F1_R(1st), R1_L(2nd), SMA_R(3rd), F2_R(4th),
607 SMA_L(5th), F1M_L(6th), F_L(7th), F1M_R(9th), F3T_R(10th), and
608 F3OP_R(11th); 4 areas belong to central regions: PRE_R(8th), 608

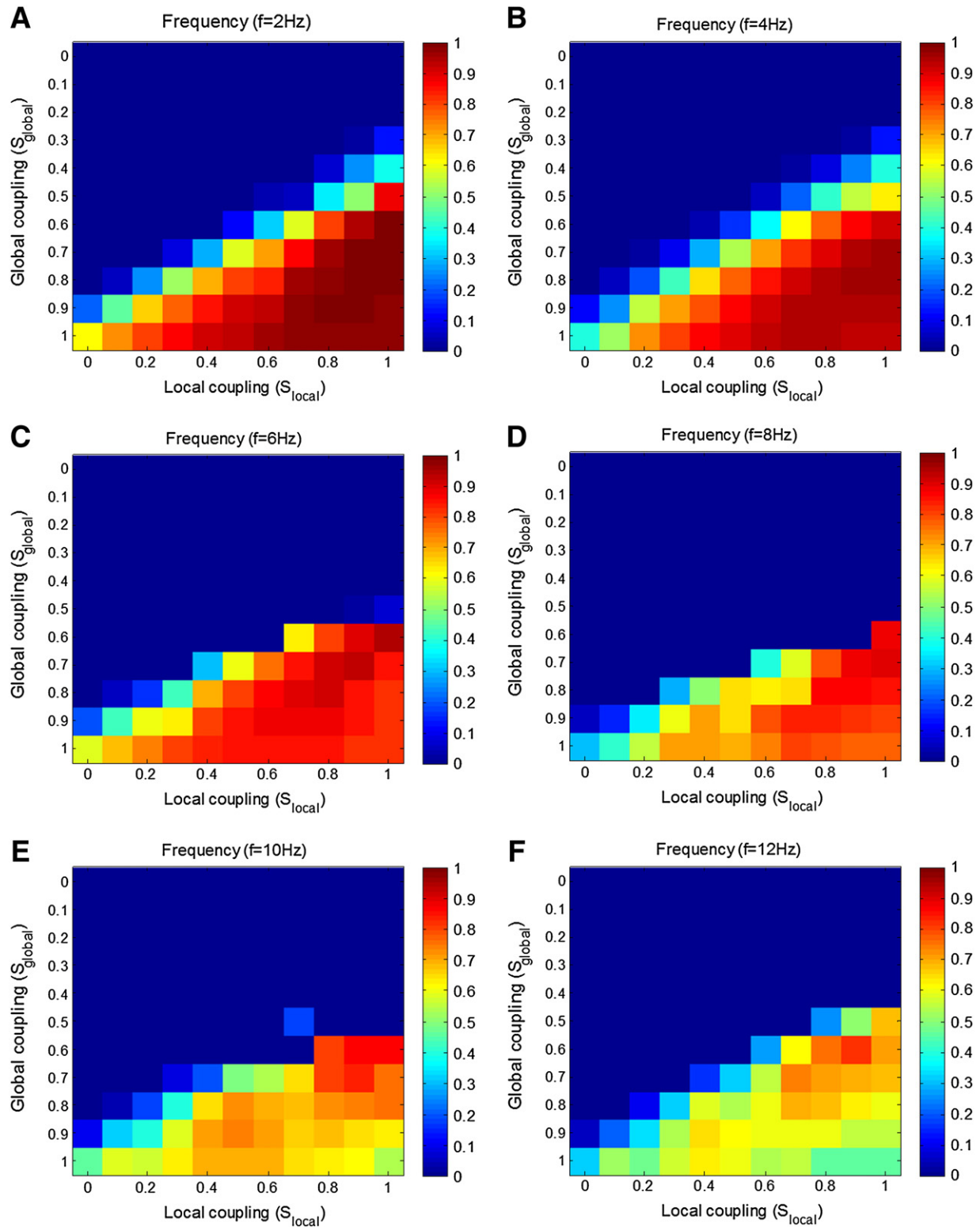


Fig. 4. Global synchronization in the parameter space of global and local coupling strength at different intrinsic frequencies. The X-axis represents the scaling factor of local coupling strength S_{local} , the Y-axis represents the scaling factor of global coupling strength S_{global} , and the color represents the amplitude of global order parameter. (A) Intrinsic frequency $f=2$ Hz. (B) Intrinsic frequency $f=4$ Hz. (C) Intrinsic frequency $f=6$ Hz. (D) Intrinsic frequency $f=8$ Hz. (E) Intrinsic frequency $f=10$ Hz. (F) Intrinsic frequency $f=12$ Hz. (For interpretation of the references to color in this figure legend, the reader is referred to the web version of the article.)

609 PRE_L(12th), POST_R(15th), and POST_L(18th); 4 areas belong to limbic
 610 lobe: MCIN_L(13th), MCIN_R(14th), ACIN_R(16th), and ACIN_L(17th);
 611 only 1 area belongs to parietal lobe: P2_L(19th); only 1 area belongs to
 612 occipital lobe: O2_L(20th). Therefore, brain areas from frontal lobe are

playing a dominant role in the initialization stage of the global syn- 613
 chronization. In addition to those frontal areas, precentral gyrus (PRE), 614
 postcentral gyrus (POST), median cingulate and paracingulate gyrus 615
 (MCIN), and anterior cingulate and paracingulate gyrus (ACIN) are also 616

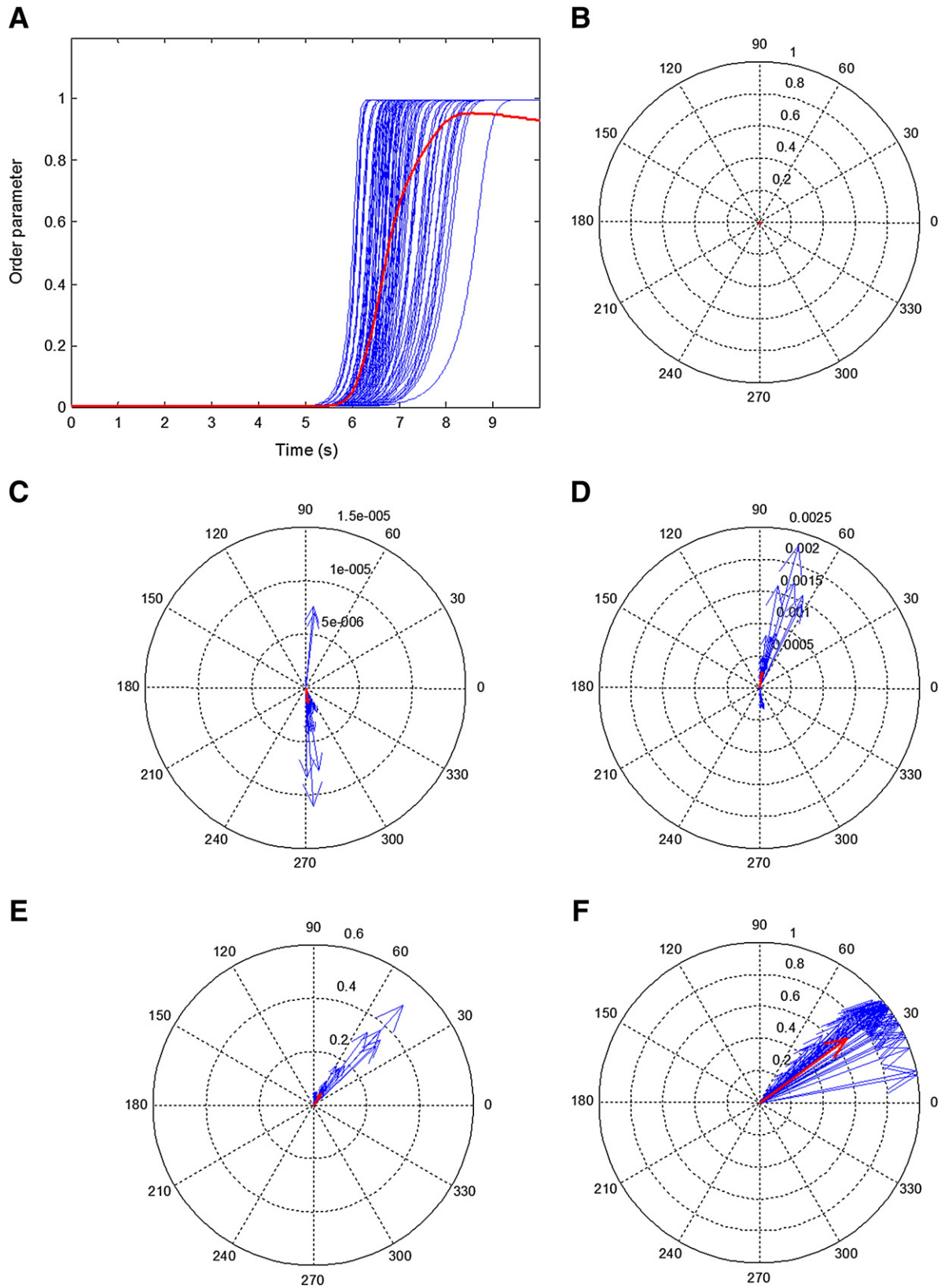


Fig. 5. The time courses of global and local synchronization. (A) The X-axis represents the time, and the Y-axis represents the amplitudes of order parameters. The blue lines represent the amplitudes of local order parameters of brain areas, and the red line represents the amplitude of the global order parameter. (B) The global (red) and local (blue) order parameters of brain areas in the polar coordinate system at $t=0$ s. (C) The global (red) and local (blue) order parameters of brain areas in the polar coordinate system at $t=4$ s. (D) The global (red) and local (blue) order parameters of brain areas in the polar coordinate system at $t=5$ s. (E) The global (red) and local (blue) order parameters of brain areas in the polar coordinate system at $t=6$ s. (For interpretation of the references to color in this figure legend, the reader is referred to the web version of the article.)

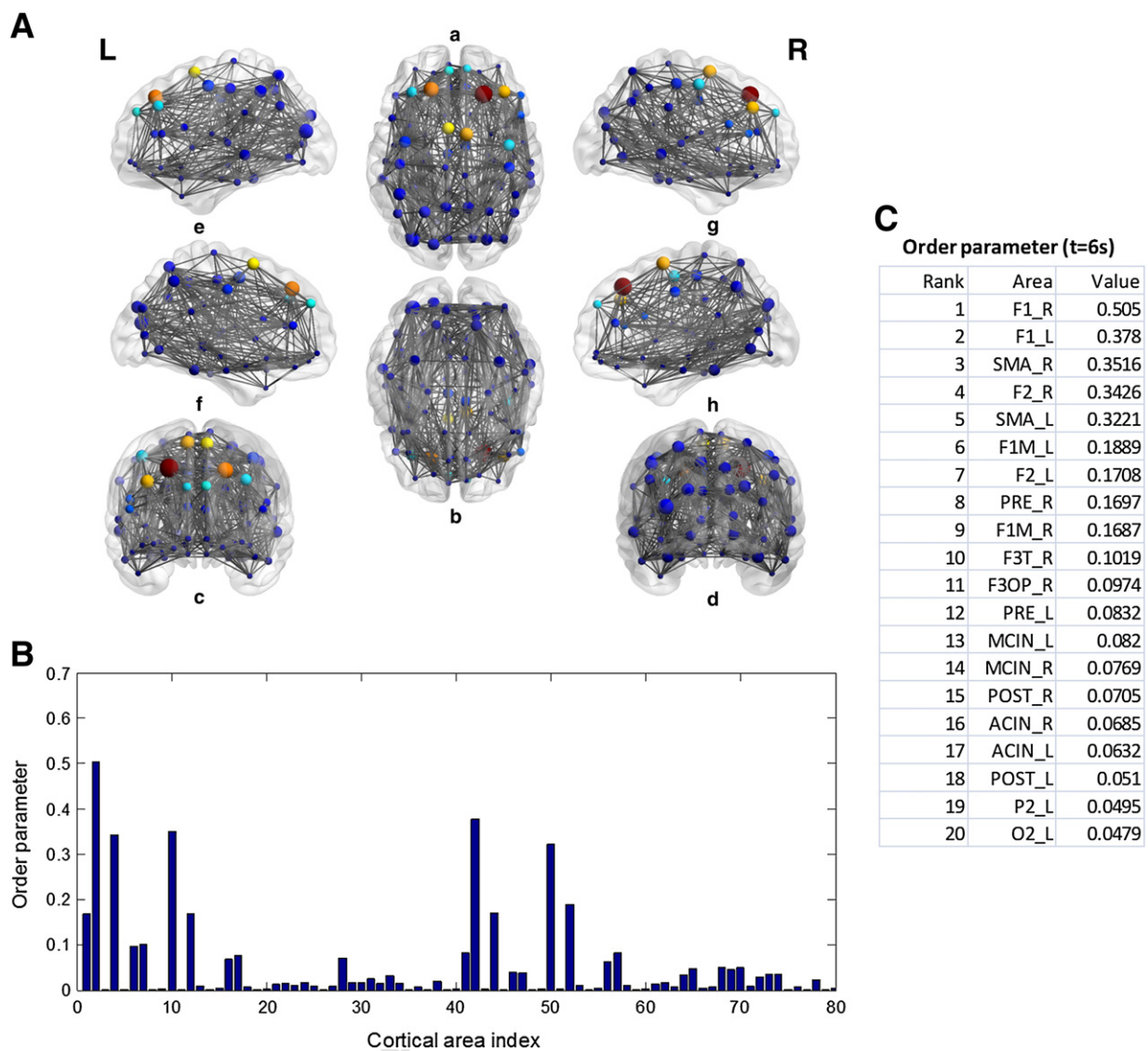


Fig. 6. Spatial distribution of local synchronization events at $t=6$ s. (A) A brain view of the amplitudes of local order parameters of brain areas. The figure includes sagittal, axial, and coronal views of both hemispheres of the brain: (a) axial top to bottom, (b) axial bottom to top, (c) coronal front to back, (d) coronal back to front, (e) sagittal left to right (left hemisphere), (f) sagittal right to left (left hemisphere), (g) sagittal right to left (right hemisphere), (h) sagittal left to right (right hemisphere). The color of nodes represents the amplitude of local order parameters (which decreases from deep red to deep blue), the size of nodes represents the degree centrality, and the size of edges connecting two nodes represents the strength of connectivity. (B) The Y-axis represents the amplitude of local order parameter and the X-axis represents the index of brain area. (C) Top twenty ranked brain areas for the amplitudes of local order parameters. (For interpretation of the references to color in this figure legend, the reader is referred to the web version of the article.)

involved in the initialization stage. Similarly, the spatial distribution of local synchronization events at $t=7$ s is shown in Fig. 7. Different from the previous case, at $t=7$ s, the amplitude of global order parameter has increased to 0.66, which means there is a substantial degree of global synchrony. In this stage, as shown in Figs. 7(A) and (B), a large number of brain areas have been fully synchronized at the local level. Among the top twenty ranked brain areas in Fig. 7(C), 9 brain areas belong to frontal lobe. While frontal areas are still dominant at this stage, there is no doubt that more and more areas from other brain regions are catching up.

Instead of the classical view of sudden generalized synchronous activities in SW epilepsy, our results are in favor of the alternative hypothesis that initiation of SW epileptic seizure originates from specific brain areas. The observation is largely in agreement with experimental studies based on brain imaging techniques (Amor et al., 2009; Holmes et al., 2004; Pavone and Niedermeyer, 2000). For example, a study by Holmes et al. (2004) used high density EEG combined with an inverse problem algorithm suggests that the initial SW had a clear anterior origin involving discrete focal regions of the frontal lobe (including dorsolateral,

orbital and cingulum areas). By graph theory analysis, we believe that the frontal focus of SW epileptic seizures can be explained by the structural connectivity as well.

Reproducibility on a biologically realistic primate brain connectivity

In this section, to show the principal findings can be replicated, we perform analysis on a biologically realistic primate brain connectivity with different parcellation. The primate brain connectivity was obtained from the CoCoMac database (Kotter, 2004), and has been successfully used to study the role of space–time structure of brain connectivity in the fluctuation of resting state networks (Ghosh et al., 2008). The connectivity matrix of a single hemisphere collated from macaque tracing studies comprises 38 nodes with weights ranging from 0 to 3.

The 36 cortical areas are listed in Fig. 8(A) (two thalamic nucleus omitted). The connectivity matrix is shown in Fig. 8(B), where connectivity strength is normalized so that the maximal strength is 1. To quantitatively explore the connectivity characteristics, we compute degree

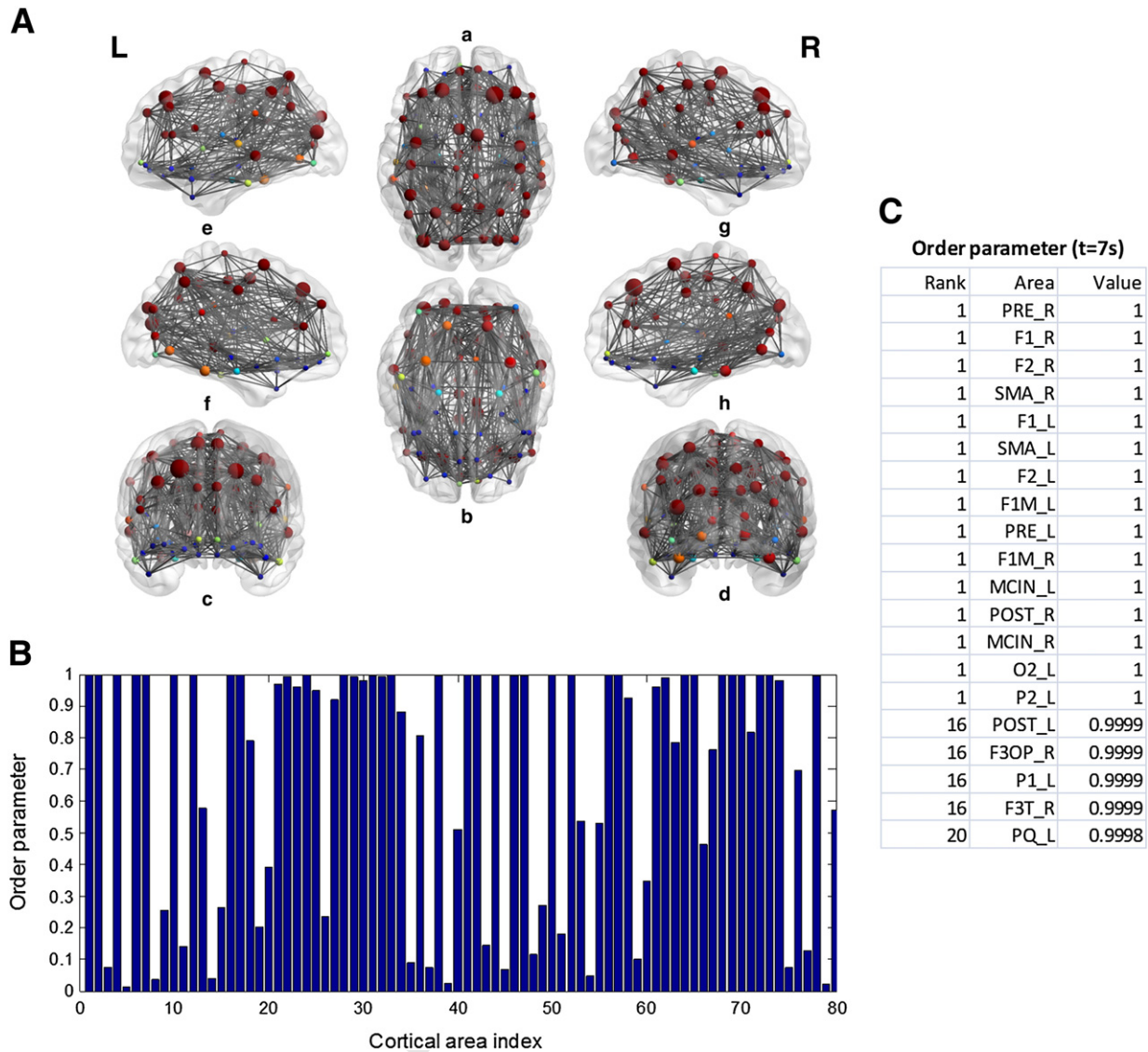


Fig. 7. Spatial distribution of local synchronization events at $t = 7$ s. (A) A brain view of the amplitudes of local order parameters of brain areas. The figure includes sagittal, axial, and coronal views of both hemispheres of the brain: (a) axial top to bottom, (b) axial bottom to top, (c) coronal front to back, (d) coronal back to front, (e) sagittal left to right (left hemisphere), (f) sagittal right to left (left hemisphere), (g) sagittal right to left (right hemisphere), (h) sagittal left to right (right hemisphere). The color of nodes represents the amplitude of local order parameters (which decreases from deep red to deep blue), the size of nodes represents the degree centrality, and the size of edges connecting two nodes represents the strength of connectivity. (B) The Y-axis represents the amplitude of local order parameter and the X-axis represents the index of brain area. (C) Top twenty ranked brain areas for the amplitudes of local order parameters. (For interpretation of the references to color in this figure legend, the reader is referred to the web version of the article.)

centrality and betweenness centrality of cortical areas, and the results are shown in the bar graphs in Figs. 8(C) and (D), respectively. The top ten brain areas for degree centrality and betweenness centrality are also listed. For degree centrality, the top five areas are PFCORB, PFCCL, PFCVL, PCIP, and TCS. For betweenness centrality, the top five areas are PFCORB, PFCCL, PCI, CCA, and TCS. Among those brain areas, PFCORB (orbital prefrontal cortex) and PFCCL (centrolateral prefrontal cortex) are highly ranked across both measures, and can be identified as structural hubs in terms of centrality.

To evaluate the temporal aspect of the coupling, the time delay between any two coupled network nodes is estimated as the ratio d/v , where d is Euclidean distance between two nodes in the three-dimensional physical space and v the propagation velocity (Ghosh et al., 2008). As realistic fiber tracking would generally result in longer pathways than the estimated shortest distance, the estimated time delay represents a lower estimate.

We demonstrate the roles of coupling strengths, time delays, and intrinsic frequencies in the emergence of global synchronization in Figs. 9(A)–(F), where X-axis represents the scaling factor of local coupling strength S_{local} , Y-axis represents the scaling factor of global coupling strength S_{global} , and the color represents the degree of global synchronization. First, to study the influence of time delays on the global synchronization, we explore the 3 dimensional subspace ($S_{global}, S_{local}, S_{delay}$) by choosing an intrinsic frequency $f = 4$ Hz. As shown in Figs. 9(A)–(C), the scaling factors of time delays are $S_{delay} = 0$ (A), $S_{delay} = 0.2$ (B), and $S_{delay} = 0.4$ (C), respectively. As the time delay increases, the degree of global synchronization is decreased. Second, to study the influence of intrinsic frequencies on the global synchronization, we explore the 3 dimensional subspace (S_{global}, S_{local}, f) by choosing a scaling factor $S_{delay} = 0.1$ for time delays. The intrinsic frequencies in Figs. 9(D)–(F) are 4 Hz, 8 Hz, and 12 Hz, respectively. It is clear that higher intrinsic frequencies have the same effects as longer time delays.

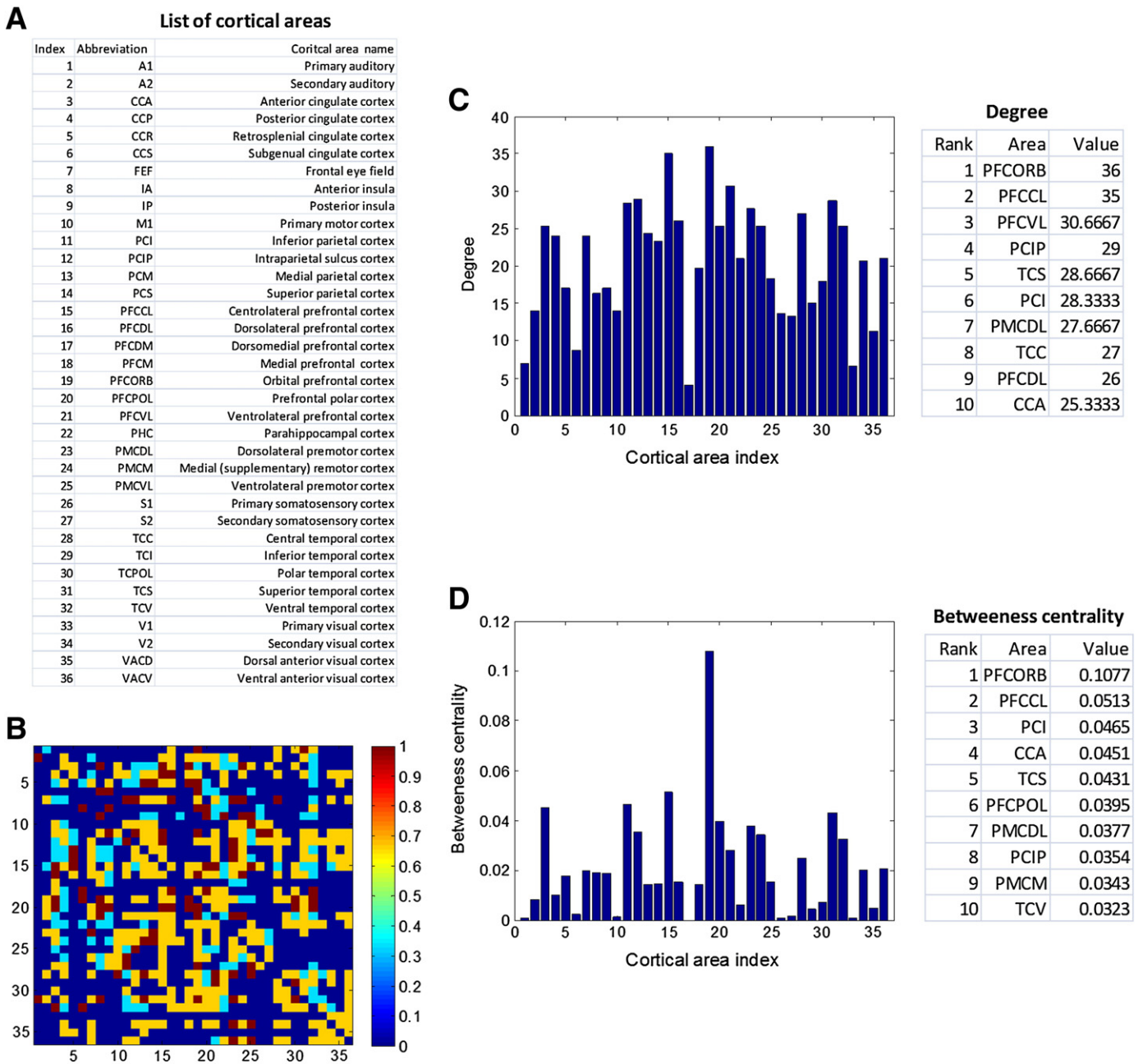


Fig. 8. Structural connectivity of the brain. (A) The list of anatomical areas of interests. There are 36 different anatomical areas of interests. In the table, each row corresponds to an anatomical area, and the columns show the index and label of the area, and the name of the area. (B) The connectivity strength matrix (the connectivity strength is normalized so that the maximal strength is 1). (C) The Y-axis represents degree centrality and the X-axis represents the index of brain area. Top ten ranked brain areas for degree centrality are listed in the table. (D) The Y-axis represents betweenness centrality and the X-axis represents the index of brain areas. Top ten ranked brain areas for betweenness centrality are listed in the table.

683 To examine the time courses of global and local synchroniza- 693
 684 tion, we choose a combination of parameter $S_{global} = 0.1$, $S_{local} = 1$, 694
 685 $S_{delay} = 0.1$, and $f = 4Hz$. As shown in Fig. 10(A), the global synchron- 695
 686 ization starts from an increase of local synchronization of some 696
 687 brain areas, and increases significantly in hundreds of milliseconds. 697
 688 The snapshots of global and local order parameters at $t = 7$ s and 698
 689 $t = 7.5$ s are shown in the polar coordinate system in Figs. 10(B) 699
 690 and (D). During early stage of initialization, at $t = 7$ s, the degree 700
 691 of synchronization is relatively small at both global and local levels. 701
 692 The maximal amplitude of local order parameters is 0.1389, and the 702

amplitude of global order parameter is 0.0775. However, by the 693
 time $t = 7.5$ s, as shown in Fig. 10(D), many brain areas have become 694
 locally synchronized, and the amplitude of global order parameter has 695
 increased substantially to 0.6256. 696

To demonstrate the correlation between the degree of local syn- 697
 chronization and the degree centrality, the amplitudes of local order 698
 parameters of brain areas at $t = 7$ s and $t = 7.5$ s are compared in 699
 Figs. 10(C)(E) and the top ten ranked brain areas are listed. In both 700
 snapshots, the top five ranked areas are PFCORB, PFCCL, PFCVL, PMCDL, 701
 and PMCM. Compared with the lists in Fig. 8, we see that the structural 702

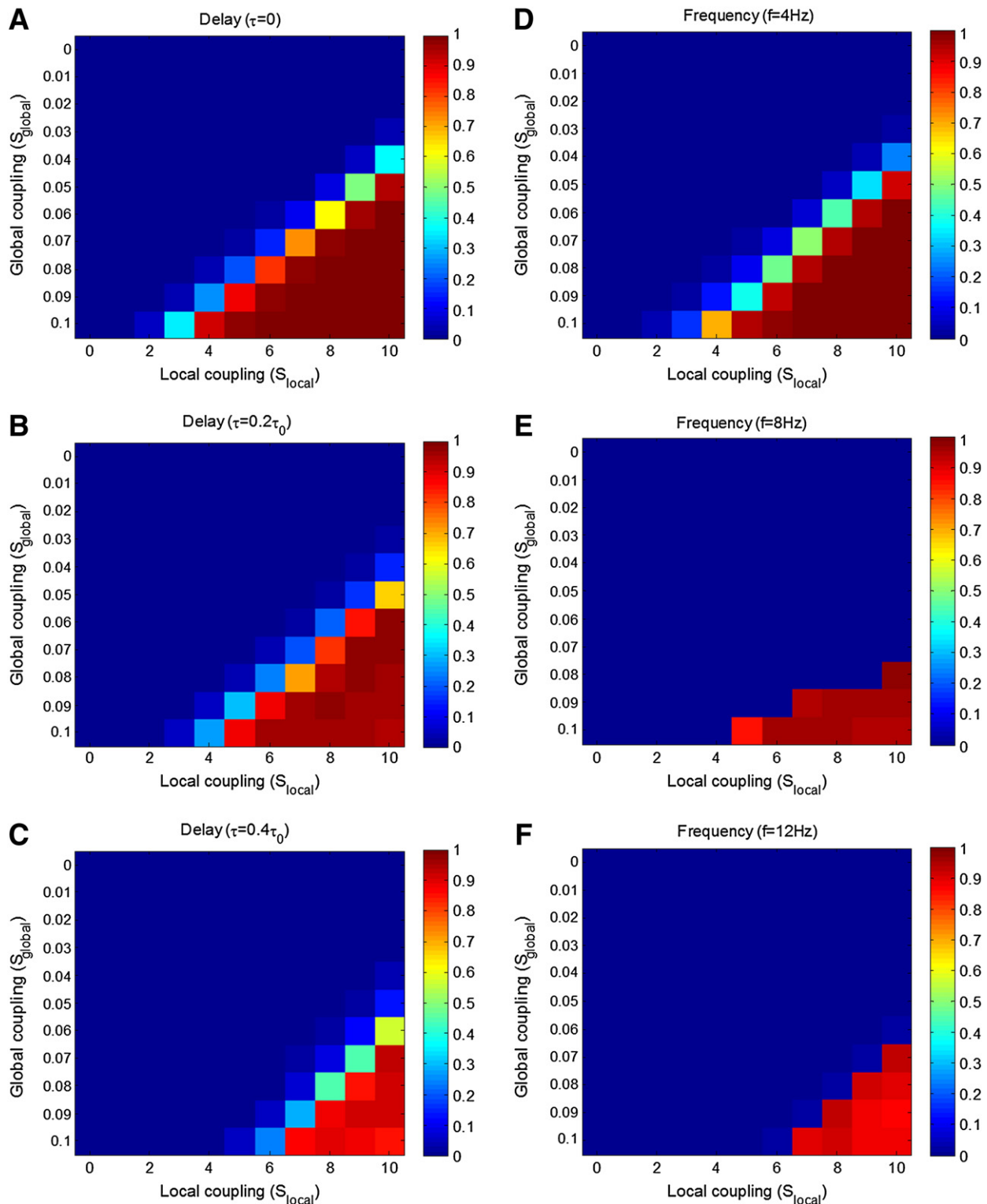


Fig. 9. Global synchronization in the parameter space of global and local coupling strength at different time delays and intrinsic frequencies. The X-axis represents the scaling factor of local coupling strength S_{local} , the Y-axis represents the scaling factor of global coupling strength S_{global} , and the color represents the amplitude of global order parameter. (A) Time delay $\tau=0$ ($v=0$ m/s) (intrinsic frequency $f=4$ Hz). (B) Time delay $\tau=0.2\tau_0$ ($v=5$ m/s) (intrinsic frequency $f=4$ Hz). (C) Time delay $\tau=0.4\tau_0$ ($v=2.5$ m/s) (intrinsic frequency $f=4$ Hz). (D) Intrinsic frequency $f=4$ Hz (time delay $\tau=0.1\tau_0$ ($v=10$ m/s)). (E) Intrinsic frequency $f=8$ Hz (time delay $\tau=0.1\tau_0$ ($v=10$ m/s)). (F) Intrinsic frequency $f=12$ Hz (time delay $\tau=0.1\tau_0$ ($v=10$ m/s)). (For interpretation of the references to color in this figure legend, the reader is referred to the web version of the article.)

703 hubs identified (PFCORB and PFCCL) are highly ranked in the lists in
 704 Fig. 10. This means global synchronization is initialized from a few “hot
 705 spots” corresponding to brain areas with highest degree of centrality.

In addition, as shown in the lists in Fig. 10, brain areas from frontal
 706 lobe are playing a dominant role in the initialization stage of the global
 707 synchronization.
 708

709 Discussion

710 The choice of the model

711 As macroscopic models are very appropriate for describing epileptic
 712 processes occurring on large-scale, those models have been widely

713 applied to explore the mechanisms underlying the EEG seizure pat-
 714 terns (Breakspear et al., 2006; Taylor and Baier, 2011; Wang et al.,
 715 2012; Wendling et al., 2002). In terms of the spike-wave discharges,
 716 an excellent example is the neural mass model proposed by the
 717 group of Lopes da Silva (Lopes da Silva et al., 2003). For a given set
 718 of parameters, the system has two simultaneous interictal and ictal

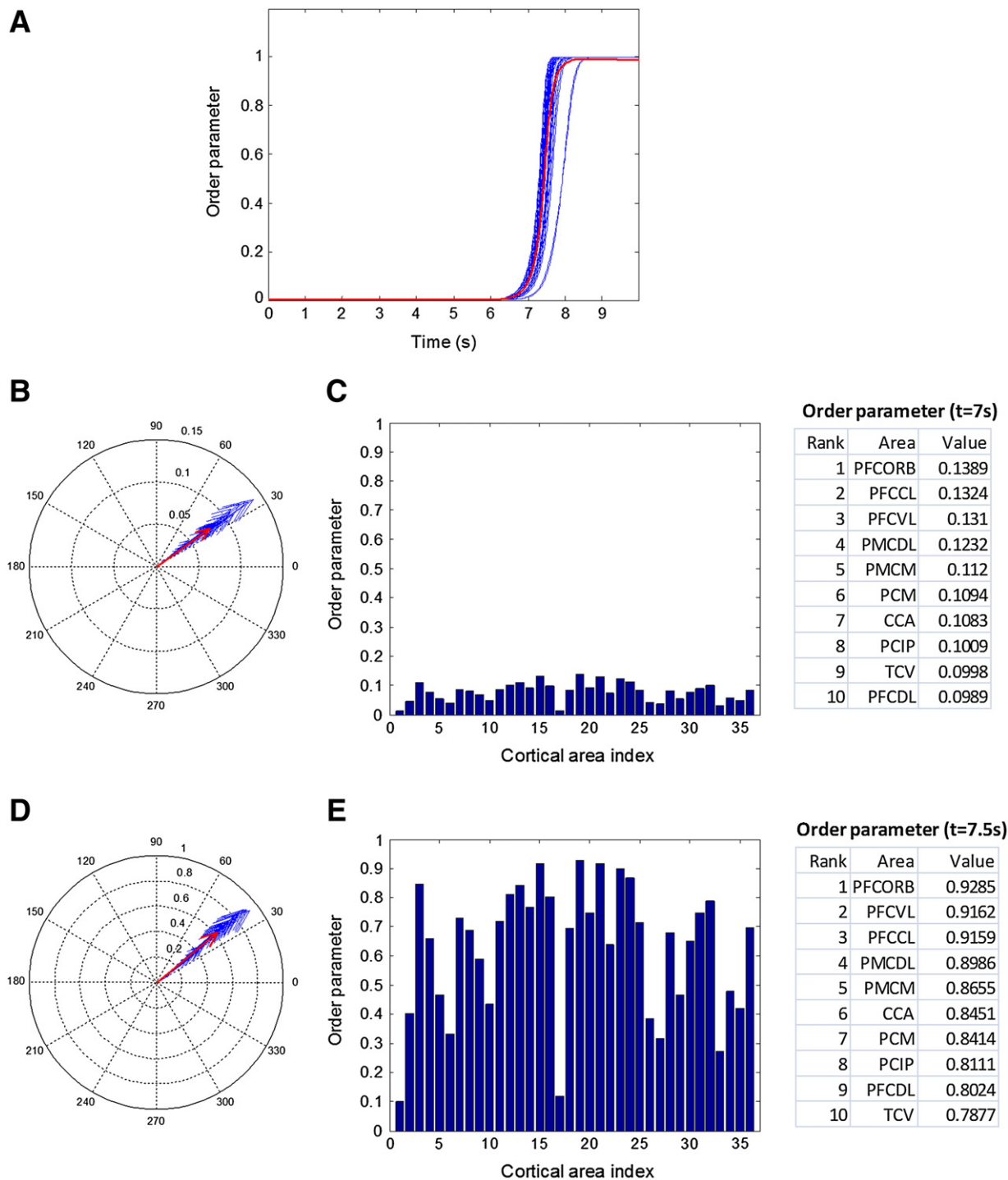


Fig. 10. The time courses of global and local synchronization. (A) The X-axis represents the time, and the Y-axis represents the amplitudes of order parameters. The blue lines represent the amplitudes of local order parameters of brain areas, and the red line represents the amplitude of the global order parameter. (B) The global (red) and local (blue) order parameters of brain areas in the polar coordinate system at $t = 7$ s. (C) The Y-axis represents the amplitude of local order parameter and the X-axis represents the index of brain area at $t = 7$ s. Top ten ranked brain areas for the amplitudes of local order parameters are listed in the table. (D) The global (red) and local (blue) order parameters of brain areas in the polar coordinate system at $t = 7.5$ s. (E) The Y-axis represents the amplitude of local order parameter and the X-axis represents the index of brain area at $t = 7.5$ s. Top ten ranked brain areas for the amplitudes of local order parameters are listed in the table. (For interpretation of the references to color in this figure legend, the reader is referred to the web version of the article.)

attractors all the time, and to which attractor the trajectories converge, depends on the initial conditions and the system's parameters. Therefore, the model shows bistability with random external input as the bifurcation parameter, and transitions between normal and seizure states are caused by the variations in the external input.

In the past five years, neural field models have been successfully used to study resting-state brain networks (Cabral et al., 2011; Deco et al., 2009, 2011; Ghosh et al., 2008; Honey et al., 2007, 2009), where simulations are performed on biologically realistic connectivity of brain areas, and the neural dynamics at each brain area is modeled by a neural mass model (FitzHugh–Nagumo oscillator, Wilson–Cowan oscillator, etc). Similarly, those neural mass models can also be used to represent the dynamics of each area in the current study. Especially, the bistable model (Lopes da Silva et al., 2003) can be a good choice to describe the dynamics of each cortical area as a bistable switch characterized by the Hopf bifurcation. In this case, there are two stable states for each cortical area: a resting point representing the normal state of the brain and a limit cycle representing the seizure state. As the neural mass model actually describes the mean activity of neuronal population, the resting point statically represents a fully desynchronized state and the limit cycle represents a fully synchronized state of each cortical area.

However, in the current study, we take a different approach. Instead of modeling each cortical area as a neural mass model, we model each cortical area by a system of coupled oscillators described by Kuramoto models. Therefore, instead of representing the activity of cortical area by a fully synchronized state or a fully desynchronized state, we are capable of quantifying the degree of synchronization of each cortical area locally as well as the whole cortex globally. This offers a better observation of the evolution of synchronization in both time and space, and thus we can clearly see if some cortical areas are more synchronized than others, or some areas are getting synchronized earlier than others.

While suitable for describing the process of synchronization, we would like to point out that the current choice of model does have limitations in exploring the initialization of SWD. Especially, the current model does not have sufficient mechanisms to reproduce the prototypic waveform of SWD.

Relationship to cellular and synaptic mechanisms

Our study has suggested that the structural connectivity may play an important role in the generation of global synchronization and thus the abnormality of white matter may contribute to the emergence of SW epileptic seizures.

The suggested structural mechanism does not contradict the proposed cellular and synaptic mechanisms (de Curtis et al., 1998; Destexhe, 1998; Destexhe et al., 1996, 1998; Dichter and Ayala, 1987; Giarretta et al., 1987; Halliwell, 1986; Pollen, 1964; Schwindt et al., 1988; Timofeev and Steriade, 2004; Timofeev et al., 2004; Wong and Prince, 1978). It is possible that the combination of mechanisms from both perspectives leads to the initialization of SW epileptic seizures. From a dynamical system point of view, intuitively, there can be two regimes in a parameter space corresponding to whether or not a global synchronization can emerge. We refer to the regime where global synchronization emerges as a pathological regime and the other as a physiological regime. The divisions of the two regimes are largely determined by structural factors. For healthy individuals, the brain structure is configured such that their “operating points” are located deeply inside the physiological regime. On the other hand, for individuals suffering from SW epilepsy, while the “operating points” are still in the physiological regime most of the time, they are located so close to the boundary such that they can be temporarily driven across the boundary under parameter perturbation. The cellular and synaptic mechanisms may be responsive for such parameter perturbation. If the structure is configured in a

way that global synchronization can easily unfold, a temporary imbalance between excitation and inhibition due to cellular and synaptic mechanisms may lead to SW epileptic seizures.

Note that, while intuitive, the above delineation of system can be too simplistic. Given the complexity of the system, it is necessary to explicitly study the role of node dynamics and network structure as an integrated whole. For example, in recent work (Gorochowski et al., 2011), a comprehensive formalism called Evolving Dynamical Network is introduced, and a new modeling framework is defined to incorporate network topology, dynamics, and evolution in an integrated way. This combination can be a potential candidate to explain the emergence of seizures because seizure generation typically involves the interplay of both node dynamics (cellular mechanisms) and network structure (synaptic connectivity).

Comparison with other experimentally inspired network studies

In fact, the abnormality of structural connectivity is often explored in a localized pathologic brain region, which is typically the focus of partial seizures. For example, in (Dyhrfeld-Johnsen et al., 2007; Santhakumar et al., 2005), the abnormal structural changes (mossy fiber sprouting, mossy cell death, etc) in dentate gyrus are studied to explore the genesis of temporal lobe epilepsy. The current study differs from those works in the following aspects.

First, different types of epilepsies are being studied. While the current work studies the emergence of abnormal hypersynchronization (related to generalized spike-wave discharges) in the anatomical structural network of human brain, the work (Dyhrfeld-Johnsen et al., 2007; Santhakumar et al., 2005) studies the genesis of temporal lobe epilepsy (a focal epilepsy). As a result, the abnormality of structural connectivity in (Dyhrfeld-Johnsen et al., 2007; Santhakumar et al., 2005) was explored in the localized pathologic region (dentate gyrus, a part of hippocampal formation). Temporal lobe epilepsy is typically believed to be related to the structural change in the anatomy of dentate gyrus. In the surgically removed hippocampus from patients with temporal lobe epilepsy, there can be major changes in the anatomy of dentate gyrus including cell death, formation of new synaptic connections as axons sprout, etc.

Second, due to the differences in the object being studied, different computational models are being used as well. The current work is based on a macroscopic model, which is more appropriate for describing epileptic processes occurring on large-scale (such as the whole brain). The work (Dyhrfeld-Johnsen et al., 2007; Santhakumar et al., 2005), on the other hand, is based on a detailed biophysical neuron network model of dentate gyrus.

White fiber abnormality

In this study, the role of brain structural connectivity in the emergence of global synchronization is examined by globally scaling the connectivity strength and fiber length matrices, which means the relative connectivity strength and fiber length between brain areas is assumed to be invariant. However, for patients with SW epileptic seizures, it is very possible that the relative connectivity strength and fiber length are varied. Recently, cross-sectional studies of children, adolescents and young adults with idiopathic generalized epilepsies (IGE) including childhood absence and juvenile myoclonic epilepsy have reported distributed patterns of abnormality predominantly affecting thalamus and frontal lobe (Betting et al., 2006a, 2006b, 2006c; Caplan et al., 2009a, 2009b; de Araujo et al., 2009; Kim et al., 2007; Pardoe et al., 2008; Pulsipher et al., 2009; Tae et al., 2006, 2008; Tosun et al., 2011). Collectively, these studies clearly indicate a neurodevelopmental contribution to anatomic abnormalities that have been observed in adults with these syndromes of epilepsy (Hermann et al., 2009). Along the same line, this may be able to explain the close relationship between absence epilepsy and

age. The fact that absence epilepsy can be outgrown might be related to the development of cortical connections, and there has been evidence suggesting that the development of cortical connections has a large influence on the coherence of brain activities. For example, a study (Thatcher et al., 2008) was conducted to explore human development of EEG coherence and phase differences over the period from infancy to 16 years of age. The results show that phase differences increase in the long inter-electrode distance as a function of age. The larger phase differences may imply that global synchronization becomes more difficult to happen as age increases. To fully shed light on this problem, more quantitative MRI studies examining patterns of brain development compared to healthy controls are needed, and it would be very interesting to carry out computational studies based on the brain connectivity of patients suffering from SW epilepsy.

859 *The characteristic frequencies of global synchronization*

860 In the past few years, existing computational studies have demon-
861 strated the important role of the characteristic “small-world” struc-
862 ture of the underlying connectivity matrix between different brain
863 areas in the spontaneous emergence of spatio-temporally structured
864 network activities (Cabral et al., 2011; Deco et al., 2009, 2011;
865 Ghosh et al., 2008; Honey et al., 2007, 2009). Especially, recent studies
866 (Cabral et al., 2011; Deco et al., 2009) have revealed that the slow
867 fluctuating and anti-correlated spatiotemporal patterns in resting
868 state are linked to fluctuations in the neural activity and synchrony
869 in the gamma range, and the most agreement occurs for a set of
870 parameters (coupling, delay, noise, etc) where subsets of brain areas
871 tend to synchronize in clusters while the network is not globally syn-
872 chronized. In this computational study, we demonstrate another as-
873 pect of structural functional relationship at different time scales:
874 while neural populations can exhibit oscillations in a wide range of
875 frequency bands, global synchronization in the brain scale only occurs
876 at low frequencies. We explain this by the interplay between time de-
877 lays associated to the structural connectivity and intrinsic frequencies
878 associated to neural populations. In this regard, we believe the low
879 characteristic frequencies of SWD are partially owing to the under-
880 lying anatomical connectivity. More interestingly, our results agree
881 with existing experimental observations: while long range synchroni-
882 zation at high frequencies (gamma rhythms) does exist in separate
883 parts of the brain (Varela et al., 2001), the scale of such synchronization
884 is quite limited compared with the generalized synchronization in SW
885 epileptic seizures. Another thing worth mentioning is that, just like
886 the resting state, global synchronization is another special case of the
887 brain state. It would be much more difficult to worth investigating to
888 explain the synchrony underlying normal brain functions in the pres-
889 ence of explicit tasks.

890 *Frontal epileptic focus*

891 By examining the interplay of local and global synchronization,
892 our results not only demonstrate that the initialization of global syn-
893 chronization has a clear anterior origin involving discrete areas of the
894 frontal lobe (including dorsolateral part of superior frontal gyrus,
895 supplementary motor area, middle frontal gyrus, etc), and but also
896 indicate that the initialized areas of global synchronization (“hot
897 spots”), correspond to the nodes with highest degree of centrality
898 (“structural hubs”). The observations of frontal focus are largely in
899 agreement with experimental studies based on brain imaging tech-
900 niques. For example, a study by Pavone showed that the origin of
901 the spike-waves is cortical with maximal frontal lobe involvement
902 (Pavone and Niedermeyer, 2000). Furthermore, a study by Holmes
903 used high density EEG combined with an inverse problem algorithm
904 to determine the location of the first SWD generators on an anatom-
905 ical MRI template. Despite inter-individual variability in the precise
906 location, the initial SWD had a clear anterior origin involving discrete

focal regions of the frontal lobe (including dorsolateral, orbital and
cingulum areas) (Holmes et al., 2004). More recently, a study by Amor
(Amor et al., 2009) explored the spatiotemporal dynamics of interac-
tions within and between widely distributed cortical sites using
magnetoencephalographic recordings of absence seizures and revealed
a multifocal fronto-central network, comprising the right prefrontal
mesial, left orbitofrontal and left lateral postcentral areas of the cortex.
While experimental observations of frontal epileptic focus do exist,
there is a lack of understanding of the underlying mechanisms. To the
best knowledge of the author, it is the first time that an explanation is
given based on a computational study with the time-space structure
of biologically realistic connectivity of 80 human cortical areas.

Note that, in the current study, all nodes are assumed to be identical
and a “hot spot” simply means a node, which becomes synchronized
earlier than others as a result of network structural connectivity. It
does not mean the node in itself is abnormal, which drives the epileptic
activity of the network. As a result, the current computational study can-
not rule out the possibility that the node in itself is also abnormal. In fact,
from a development point of view, due to some seizure induced changes,
a normal node may also become abnormal if the network structure
makes it always the starting point of seizures.

Acknowledgments

We thank Andrew Zalesky and Alex Fornito for the structural data
for human brain connectivity.

References

- Acebron, J.A., 2005. The Kuramoto model: a simple paradigm for synchronization phenomena. *Rev. Mod. Phys.* 77 (1), 137–185 (Jan).
- Amor, F., Baillet, S., Navarro, V., Adam, C., Martinierie, J., Quyen, M.L.V., 2009. Cortical local and long-range synchronization interplay in human absence seizure initiation. *NeuroImage* 45, 950–962.
- Arenas, A., Diaz-Guilera, A., Kurths, J., Moreno, Y., Zhou, C., 2008. Synchronization in complex networks. *Phys. Rep.* 469 (3), 93–153.
- Benjamin, O., Fitzgerald, T.H.B., Ashwin, P., Tsaneva-Atanasova, K., Chowdhury, F., Richardson, M.P., Terry, J.R., 2012. A phenomenological model of seizure initiation suggests network structure may explain seizure frequency in idiopathic generalized epilepsy. *J. Math. Neurosci.* 2, 1 <http://dx.doi.org/10.1186/2190-8567-2-1>.
- Betting, L.E., Mory, S.B., Li, L.M., Lopes-Cendes, I., Guerreiro, M.M., Guerreiro, C.A.M., Cendes, F., 2006a. MRI reveals structural abnormalities in patients with idiopathic generalized epilepsy. *Neurology* 67, 848–852.
- Betting, L.E., Mory, S.B., Li, L.M., Lopes-Cendes, I., Guerreiro, M.M., Guerreiro, C.A.M., Cendes, F., 2006b. MRI volumetry shows increased anterior thalamic volumes in patients with absence seizures. *Epilepsy Behav.* 8, 575–580.
- Betting, L.E., Mory, S.B., Li, L.M., Lopes-Cendes, I., Guerreiro, M.M., Guerreiro, C.A.M., Cendes, F., 2006c. Voxel-based morphometry in patients with idiopathic generalized epilepsies. *NeuroImage* 32, 498–502.
- Breakspear, M., Roberts, J.A., Terry, J.R., Rodrigues, S., Mahant, N., Robinson, P.A., 2006. A unifying explanation of primary generalized seizures through nonlinear brain modeling and bifurcation analysis. *Cereb. Cortex* 16, 1296–1313.
- Breakspear, M., Heitmann, S., Daffertshofer, A., 2010. Generative models of cortical oscillations: neurobiological implications of the Kuramoto model. *Front. Hum. Neurosci.* 4, 190 <http://dx.doi.org/10.3389/fnhum.2010.00190> (Nov).
- Cabral, J., Hugues, E., Sporns, O., Deco, G., 2011. Role of local network oscillations in resting-state functional connectivity. *Front. Hum. Neurosci.* 1 (57), 130–139 (Jul).
- Caplan, R., Levitt, J., Siddarth, P., Wu, K.N., Gurbani, S., Sankar, R., Shields, W.D., 2009a. Frontal and temporal volumes in childhood absence epilepsy. *Epilepsia* 50 (11), 2466–2472.
- Caplan, R., Levitts, J., Siddarth, P., Wu, K.N., Gurbani, S., 2009b. Language and fronto-temporal volumes in pediatric epilepsy. *Epilepsy Behav.* 17 (3), 402–407.
- de Araujo, G.M., Jackowski, A.P., Lin, K., Guaranha, M.S.B., Guilhoto, L.M.F.F., da Silva, H.H., Caboclo, L.O.S.F., Garrete, H., Bressan, R.A., Yacubian, E.M.T., 2009. Personality traits related to juvenile myoclonic epilepsy: MRI reveals prefrontal abnormalities through a voxel-based morphometry study. *Epilepsy Behav.* 15 (2), 202–207.
- de Curtis, M., Radici, C., Forti, M., 1998. Cellular mechanisms underlying spontaneous interictal spikes in an acute model of focal cortical epileptogenesis. *Neuroscience* 88, 107–117.
- Deco, G., Jirsa, V.K., McIntosh, A.R., Sporns, O., Kotter, R., 2009. Key role of coupling, delay, and noise in resting brain fluctuations. *Proc. Natl. Acad. Sci.* 106 (25), 10302–10307 (June).
- Deco, G., Jirsa, V.K., McIntosh, A.R., 2011. Emerging concepts for the dynamical organization of resting-state activity in the brain. *Nat. Rev. Neurosci.* 12, 43–56 (Jan.).
- Destexhe, A., 1998. Spike-and-wave oscillations based on the properties of GABA(B) receptors. *J. Neurosci.* 18, 9099–9111.

- 979 Destexhe, A., Bal, T., McCormick, D.A., Sejnowski, T.J., 1996. Ionic mechanisms underlying
980 synchronizing oscillations and propagating waves in a model of ferret thalamic
981 slices. *J. Neurophysiol.* 76, 2049–2070.
- 982 Destexhe, A., Contreras, D., Steriade, M., 1998. Mechanisms underlying the synchronizing
983 action of corticothalamic feedback through inhibition of thalamic relay cells.
984 *J. Neurophysiol.* 79, 999–1016.
- 985 Dichter, M.A., Ayala, G.F., 1987. Cellular mechanisms of epilepsy: a status report. *Science*
986 237, 157–164.
- 987 Dyhrfeld-Johnsen, J., Santhakumar, V., Morgan, R.J., Huerta, R., Tsimring, L., Soltesz,
988 I., 2007. Topological determinants of epileptogenesis in large-scale structural
989 and functional models of the dentate gyrus derived from experimental data.
990 *J. Neurophysiol.* 97, 1566–1587.
- 991 Ghosh, A., Rho, Y., McIntosh, A.R., Kotter, R., Jirsa, V.K., 2008. Noise during rest enables
992 the exploration of the brain's dynamic repertoire. *PLoS Comput. Biol.* 4 (10), e1000196
993 <http://dx.doi.org/10.1371/journal.pcbi.1000196> (Oct.).
- 994 Giaretta, D., Avoli, M., Gloor, P., 1987. Intracellular recordings in pericruciate neurons
995 during spike and wave discharges of feline generalized penicillin epilepsy. *Brain*
996 Res. 405, 68–79.
- 997 Goodfellow, M., Schindler, K., Baier, G., 2011. Intermittent spike-wave dynamics in a
998 heterogeneous, spatially extended neural mass model. *NeuroImage* 55, 920–932.
- 999 Gorochowski, T.E., Bernardo, M.D., Grierson, C.S., 2011. Evolving dynamical networks: a
1000 formalism for describing complex systems. *Complexity* 17 (3), 18–25.
- 1001 Halliwell, J.V., 1986. M-current in human neocortical neurones. *Neurosci. Lett.* 67 (1),
1002 1–6.
- 1003 Hermann, B.P., Jones, J.J., Jones, J.E., Seidenberg, M., 2009. The emerging architecture of
1004 neuropsychological impairment in epilepsy. *Neurol. Clin.* 27 (4), 881–907.
- 1005 Holmes, M.D., Brown, M., Tucker, D.M., 2004. Are generalized seizures truly generalized?
1006 Evidence of localized mesial frontal and frontopolar discharges in absence. *Epilepsia*
1007 45 (12), 1568–1579.
- 1008 Honey, C.J., Kotter, R., Breakspear, M., Sporns, O., 2007. Network structure of cerebral
1009 cortex shapes functional connectivity on multiple time scales. *Proc. Natl. Acad. Sci.*
1010 104 (24), 10240–10245 (Jun.).
- 1011 Honey, C.J., Sporns, O., Cammoun, L., Gigandet, X., Thiran, J.P., Meuli, R., Hagmann, P.,
1012 2009. Predicting human resting-state functional connectivity from structural con-
1013 nectivity. *Proc. Natl. Acad. Sci.* 106 (6), 2035–2040 (Feb.).
- 1014 Kim, J.H., Lee, J.K., Koh, S.B., Lee, S.A., Lee, J.M., Kim, S.I., Kang, J.K., 2007. Regional grey
1015 matter abnormalities in juvenile myoclonic epilepsy: a voxel-based morphometry
1016 study. *NeuroImage* 37 (4), 1132–1137.
- 1017 Kitzbichler, M.G., Smith, M.L., Christensen, S.R., Bullmore, E., 2009. Broadband criticality
1018 of human brain network synchronization. *PLoS Comput. Biol.* 5 (3), e1000314
1019 <http://dx.doi.org/10.1371/journal.pcbi.1000314>.
- 1020 Kotter, R., 2004. Online retrieval, processing, and visualization of primate connectivity
1021 data from the CoCoMac database. *Neuroinformatics* 2, 127–144.
- 1022 Kuramoto, Y., 1984. *Chemical Oscillations, Waves and Turbulence*. Springer, New York.
- 1023 Lopes da Silva, F.H., Blanes, W., Kalitzin, S.N., parra, J., Suffczynski, P., Velis, D.N., 2003.
1024 Dynamical diseases of brain systems: different routes to epileptic seizures. *IEEE*
1025 *Trans. Biomed. Eng.* 50, 540–548.
- 1026 Lytton, W.W., 2008. Computer modelling of epilepsy. *Nat. Rev. Neurosci.* 9, 626–637
1027 (Aug.).
- 1028 Pardoe, H., Pell, G.S., Abbott, D.F., Berg, A.T., Jackson, G.D., 2008. Multi-site voxel-based
1029 morphometry: methods and a feasibility demonstration with childhood absence
1030 epilepsy. *NeuroImage* 42 (2), 611–616.
- 1031 Pavone, A., Niedermeyer, E., 2000. Absence seizures and the frontal lobe. *Clin. Electroencephalogr.*
1032 31 (3), 153–156 (Jul.).
- Pollen, D.A., 1964. Intracellular studies of cortical neurons during thalamic induced
1033 wave and spike. *Electroencephalogr. Clin. Neurophysiol.* 17, 398–404. 1034
- Pulsipher, D.T., Seidenberg, M., Guidotti, L., Tuchscherer, V.N., Morton, J., Sheth, R.D.,
1035 Hermann, B., 2009. Thalamofrontal circuitry and executive dysfunction in recent-
1036 onset juvenile myoclonic epilepsy. *Epilepsia* 50 (5), 1210–1219. 1037
- Rubinov, M., Sporns, O., 2010. Complex network measures of brain connectivity: uses
1038 and interpretations. *NeuroImage* 52, 1059–1069. 1039
- Santhakumar, V., Aradi, I., Soltesz, I., 2005. Role of mossy fiber sprouting and mossy cell
1040 loss in hyperexcitability: a network model of the dentate gyrus incorporating cell
1041 types and axonal topography. *J. Neurophysiol.* 93, 437–453. 1042
- Schwindt, P.C., Spain, W.J., Foehring, R.C., Stafstrom, C.E., Chubb, M.C., Crill, W.E., 1988.
1043 Multiple potassium conductances and their functions in neurons from cat sensori-
1044 motor cortex in vitro. *J. Neurophysiol.* 59, 424–449. 1045
- Tae, W.S., Hong, S.B., Joo, E.Y., Han, S.J., Cho, J.W., Seo, D.W., Lee, J.M., Kim, I.J., Byun, H.S.,
1046 Kim, S.I., 2006. Structural brain abnormalities in juvenile myoclonic epilepsy patients:
1047 volumetry and voxel-based morphometry. *Korean J. Radiol.* 7 (3), 162–172. 1048
- Tae, W.S., Kim, S.H., Joo, E.Y., Han, S.J., Kim, I.Y., Kim, S.I., Lee, J.M., Hong, S.B., 2008.
1049 Cortical thickness abnormality in juvenile myoclonic epilepsy. *J. Neurol.* 255 (4),
1050 561–566. 1051
- Taylor, P.N., Baier, G., 2011. A spatially extended model for macroscopic spike-wave
1052 discharges. *J. Comput. Neurosci.* 31, 679–684. 1053
- Terry, J.R., Benjamin, Q., Richardson, M.P., 2012. Seizure generation: the role of nodes
1054 and networks. *Epilepsia* <http://dx.doi.org/10.1111/j.1528-1167.2012.03560.x>. 1055
- Thatcher, R.W., North, D.M., Biver, C.J., 2008. Development of cortical connections as
1056 measured by EEG coherence and phase delays. *Hum. Brain Mapp.* 29, 1400–1415. 1057
- Timofeev, I., Steriade, M., 2004. Neocortical seizures: initiation, development and cessa-
1058 tion. *Neuroscience* 123, 299–336. 1059
- Timofeev, I., Grenier, F., Steriade, M., 2004. Contribution of intrinsic neuronal factors in
1060 the generation of cortically driven electrographic seizures. *J. Neurophysiol.* 92,
1061 1138–1143. 1062
- Tosun, D., Dabbs, K., Caplan, R., Siddarth, P., Toga, A., Seidenberg, M., Hermann, B., 2011.
1063 Deformation-based morphometry of prospective neurodevelopmental changes in
1064 new onset paediatric epilepsy. *Brain* 134 (4), 1003–1014 (April). 1065
- Tzourio-Mazoyer, N., Landeau, B., Papathanassiou, D., Crivello, F., Etard, O., Delcroix, N.,
1066 Mazoyer, B., Joliot, M., 2002. Automated anatomical labeling of activations in SPM
1067 using a macroscopic anatomical parcellation of the MNI MRI single-subject brain.
1068 *NeuroImage* 15 (1), 273–289 (Jan). 1069
- Uhlhaas, P.J., Singer, W., 2006. Neural synchrony in brain disorders: relevance for cog-
1070 nitive dysfunctions and pathophysiology. *Neuron* 52, 155–168. 1071
- Varela, F., Lachaux, J., Rodriguez, E., Martinerie, J., 2001. The brainweb: phase synchroni-
1072 zation and large-scale integration. *Nat. Rev. Neurosci.* 2 (4), 229–239. 1073
- Wang, Y., Goodfellow, M., Taylor, P.N., Baier, G., 2012. Phase space approach for
1074 modeling of epileptic dynamics. *Phys. Rev. E* 85 (6) <http://dx.doi.org/10.1103/PhysRevE.85.061918>. 1075
- Wendling, F., Bartolomei, F., Bellanger, J.J., Chauvel, P., 2002. Epileptic fast activity
1076 can be explained by a model of impaired GABAergic dendritic inhibition. *Eur. J. Neurosci.*
1077 15 (9), 1499–1508. 1078
- Wong, R.K., Prince, D.A., 1978. Participation of calcium spikes during intrinsic burst
1080 firing in hippocampal neurons. *Brain Res.* 159 (2), 385–390. 1081
- Yan, B., Li, P., 2011. An integrative view of mechanisms underlying generalized spike-
1082 and-wave epileptic seizures and its implication on optimal therapeutic treatments.
1083 *PLoS One* 6 (7), e22440 <http://dx.doi.org/10.1371/journal.pone.0022440> (July). 1084
- Zalesky, A., Fornito, A., 2009. A DTI-derived measure of cortico-cortical connectivity.
1085 *IEEE Trans. Med. Imaging* 28 (7), 1023–1036 (Jul.). 1086